Optical Tuning of the Whispering Gallery Modes of a Silicon Microsphere

by

Imran Khan

A Thesis submitted to the

Graduate School of Sciences and Engineering

in partial fulfillment of the requirements for

the Degree of

Master of Science

in

Optoelectronics and Photonics Engineering

Koç University

September 2015

Koç University

Graduate School of Sciences and Engineering

This is to certify that I have examined this copy of a master's thesis by

Imran Khan

and have found that it is complete and satisfactory in all respects,

and that any and all revisions required by the final

examining committee have been made.

Committee Members:

_____

Ali Serpengüzel, Ph. D. (Advisor)

_____

Erdem Alaca, Ph. D.

_____

Erdal Bulgan, Ph. D.

Date: _____

Abstract

Silicon, being a choice for semiconductor industry for past many decades has shown great importance in integrating photonics with complementary metal oxide semiconductor (CMOS) technology. Additionally in recent years, whispering gallery mode (WGM) resonators have been studied extensively for many photonics applications like optical filters, modulators, resonators, amplifiers, and phase shifters. WGM resonators can also be used towards realization of all optical functional devices. Here, in this work, we have performed the optical tuning of WGMs of a silicon microsphere of radius 500 μm at 1427 nm. The optical tuning of the WGMS is achieved by modulating the refractive index of the silicon with a pump laser at 405 nm, causing a red shift of the WGMs. WGMs with a mode spacing of $\Delta\lambda = 0.23$ nm and quality factors of ~60000 have been observed. For an unfocused continuous wave (CW) pump illumination at 405 nm, a red shift of 13.5 pm, and with focused pump laser beam, a red shift of 24.5 pm is observed. Further, a red shift of 40 pm is observed, when an unfocused 8 Hz 80% duty cycle pulsed pump laser is applied to the silicon microsphere. The observed red shift in the WGMs is due to the thermo-optical effect in silicon in response to slow modulation of the refractive index of silicon by the pump laser.

Keywords: Optical resonators, silicon, switching, thermal effects, whispering gallery modes

Özet

Geçtiğimiz yüzyılda silisyum, yarıiletken üretimi için taban bileşen olmuş, ve fotonik alanında da CMOS teknolojisi ile birlikte kullanılacağı öngörülmüştür. Ayrıca son yıllarda fısıldayan geçit kipli (FGK) optik çınlaçları; optik süzgeçler, kipleyiciler, yükselticiler, ve evre yöneticileri gibi çeşitli fotonik uygulamalarında yer bulmuştur. FGK çınlaçları tümleşik optik aygıtların üretiminde yer alabilir. Bu tezde, 1427 nm dalgaboyunda çalışan bir lazerle 500 μm yarıçaplı silisyum mikroyuvarların FGK'lerinin optik izge ayarlaması çalışılmıştır. FGK çınlaçları 405 nm'de çalışan bir uyarı lazeri ile silisyum yuvarın kırılma katsayısını değiştirerek kırmızıya kaydırılmıştır. Kip aralığı $\Delta\lambda = 0.23$ nm ve nitelik katsayısı $Q \approx 60000$ olan FGK'ler gözlemlenmiştir. Bu adımdan sonra uyarı lazeriyle ölçümlere geçilmiştir. Bu deneylerde, 405 nm dalgaboyunda çalışan ve odaklı olmayan sürekli dalga (SD) odaklanmamış uyarı lazeri kullanılarak silisyum yuvar FGK izgesinde 13.5 pm, ve odaklı uyarı lazeri kullanıldığında ise 24.5 pm kırmızıya kayma gözlemlenmiştir. Ek olarak, uyarı lazeri 8 Hz sıklığında % 80 çevrim ile odaksız kullanıldığında FGK kiplerinde 40 pm'ye kadar kırmızıya kayma gözlemlenmiştir. Silisyum yuvarın FGK'lerinde gözlenen kırmızıya kayma uyarma lazeriyle ısıl-optik olarak optik kırılma katsayısının artırılmasıyla elde edilmiştir.

Acknowledgments

I would like to thank and express my deepest gratitude to my MSc thesis advisor Professor Ali Serpengüzel for his support, guidance, motivation and patience during my M.Sc. studies at Koç University Microphotonics Research Laboratory. Without him I would not have been be able to perform this work. I thank him for sharing his vision and experience in the field of photonics, and making it easy for me to learn many great things in just two years. I would like to thank my MSc thesis committee members Assoc. Prof. Dr. Erdem Alaca and Asst. Prof. Dr. Erdal Bulgan for their critical reading of my thesis and their constructive comments.

I would like to thank Dr. Ulaş Sabahattin Gökay for his training, guidance and friendship. I learnt a lot from his experience and knowledge in optical resonators, and Mr. Selçuk Çakmak for his technical support throughout the two years in the experiments. I also thank Muhammad Hamza Humayun and Muhammad Zakwan for their valuable discussions and help at Koç University Microphotonics Research Laboratory.

I dedicate this thesis to my family, specially to (Ammi and Khan-g), who always showed the best care, love, and support in my entire life till this time. I am so proud of having such beautiful and lovely parents. I also would like to mention my precious friend, my sister for her support and prayers.

I would like to thank my best buddies Qamer Uddin and Muhsin Ali, who always shared my good and bad times, and making our friendship the best in the world.

I thank my friends Ismail Yorulmaz, Abdullah Muti, Mustafa Eryürek, Abdullah Bilgin, Andleeb Zahra, Adil Abbas, and Talha Irfan Khan for making my stay in Istanbul a great experience. I am specifically thankful to Ismail Yorulmaz for his great friendship, support and help during the past

more than one year. I would like to acknowledge Ismail Yorulmaz and Işınsu Baylam for arranging pump laser power measurements at Koç University Laser Research Laboratory.

I would also like to thank Koç University Surface Technologies and Application Research Center and would like to acknowledge Türkiye Bilimsel ve Teknolojik Araştırma Kurumu (TÜBİTAK) grant No: 114F312 for the partial financial support to our research.

And finally, I would like to say thank to my housemates Talha Köseoğlu and Burak Gökgür for making our stay at Emlak B13:10 memorable, lovely and enjoyable. I will miss you guys.

Table of Contents

List of Tables

List of Figures

Nomenclature

a	Radius of the microsphere
b	Impact parameter
c	Speed of light in vacuum
$j_n(x)$	Spherical Bessel function
$h_n^{(2)}(x)$	Hankel function of Second kind
k	Propagation vector
l	Radial mode order
m	Azimuthal mode number
m_{ce}^*	Effective mass of the electrons
m_{ch}^*	Effective mass of holes
n	Polar angular mode number
N_{sph}	Refractive index of the sphere
N_o	Refractive index of the outside medium
dN/dT	Thermo-optic effect coefficient
P	Polarization
Q	Quality factor

Q_{ext}	Extinction efficiency quality factor
Q_{sca}	Scattering efficiency quality factor
Q_{ss}	Surface scattering quality factor
T	Temperature
V	Volume
x	Size parameter
α_{FC}	Free carrier absorption coefficient
α_m	Polarizability
λ	Wavelength of the light in vaccum
$\Delta\lambda$	Change in resonance wavelength
$\delta\lambda$	Polar mode spacing
ε	Dielectric function
τ	Photon lifetime in cavity
ω_α	Resonance angular frequency
χ	Dielectric susceptibility

Chapter 01

INTRODUCTION

1.1 Silicon Photonics

Silicon (Si) has been a choice for the semiconductor industry for the past couple of decades has shown great importance in integrating photonics with complementary metal oxide semiconductor (CMOS) technology, which offers advantages like reliable manufacturing at micro/nano scale and with low cost. The compatibility with CMOS technology allows for optoelectronics integration on the same chip, which offers solutions to high speed and high data rate bottlenecks in communication systems.

Silicon has attracted our attention for its potential use in future light based technologies [1] [2] [3], since Si is abundantly available in nature, the bandgap of 1.12 eV offers transparent behavior to telecommunication wavelengths (1270-1625) nm, which allows one the manipulation of light. The bulk silicon limits the potential use of silicon in optoelectronics integration, because of its indirect bandgap which makes it inefficient emitter of photons. Thanks to nanotechnology for addressing this issue in the form of nanostructures [4], by which the very low radiative recombination could be overcome by introducing impurity to engineer the bandgap. Further the study of optical properties of amorphous and crystalline silicon yields that, crystalline silicon can enhance the absorption in a broad spectral range, i.e., visible and near-IR region, and also by changing the crystal size bandgap can be engineered [5]. Amorphous silicon possess much higher absorption in the region between 400-800 nm [6] with additional feature of providing

passivation of the surface defects, which are important for realizing efficient high electronic mobilities. Porous silicon also exhibits nonlinear properties, which can be used in solar cells and light emitting devices [7].

Additionally, silicon shows excellent material properties like high thermal conductivity (~10 higher than GaAs), high optical damage threshold (~10 higher than GaAs), and high third order non-linearity (the Kerr effect is 100 times larger and the Raman effect is 1000 times larger than those in silica) [1], which makes Si an ideal candidate for the realization of all optical systems.

So as a dominant material in the electronics industry for many decades and the second most abundantly available material in the Earth's crust [8], silicon has a potential future for the photonics industry as well. The maturity of silicon in the integrated circuit (IC) industry along with its highest crystal quality of any semiconductor provides motivation for silicon photonics.

1.2 Optical resonators in silicon photonics

Crystalline silicon, used for waveguiding, modulating, emitting and switching infrared light with different resonators structures like disks and rings [9] [10] has already paved the way to realization of various micro cavity resonators. Numerous work has been done in all optical control of light in Si resonant cavities [11] [12]. The efficiency of weak optical effects in Si be enhanced due to confinement of intensity and phase inside these cavities. Resonant optical cavities are characterized by modes, which are localized as the confined light with a defined photon lifetime. Among the possible cavity structures are microspheres [13], microdisks and microrings [14], microtoroids [15] have commonly been investigated and optical phenomena like switching, modulating, and filtering have been demonstrated.

All optical switching and modulation in silicon has been demonstrated [16] [17] with long and large structures, which poses limitations for on chip integration of components. All optical switching in a silicon ring resonator of micrometer size [18], and a low loss and high quality factor 10^7 microring resonator [19] has been shown experimentally. Also a silicon microring resonator with quality factor of 5×10^5 [20], and a silicon microring for the study of entangled photon pairs [21] have been demonstrated. A silicon core silica clad microspherical resonator for exploiting large wavelength shifts based on Kerr nonlinearity [22] has recently been demonstrated. In another work, the fabrication of a silicon microdisk, which exhibits a quality factor of 3×10^6 [23] has been shown.

1.3 Work Outline

This work is based on whispering gallery modes (WGMs) of a silicon (Si) microsphere. More specifically, we show the tuning of the WGMs of a silicon microsphere of radius 500 μm at 1428 nm central wavelength (probe laser) by changing the refractive index of the sphere by a GaN 405 nm laser (pump laser), for the first time to the best of our knowledge. The physical effect attributed for this work is thermo-optic effect (TOE), where millisecond regime pulses create a thermal change in the refractive index of the silicon microsphere and red shift the resonance spectra. We have performed the pump excitation in both continuous wave (CW) and pulsed modes.

Chapter 2 discusses the optical effects in silicon. An overview is first given about changing the refractive index of silicon by all optical or electro-optic pump excitation. The effects which cause a change in the refractive index of a material are thermo-optic effect (TOE), Kerr effect, one photon absorption (OPA), two photon absorption (TPA), free carrier absorption (FCA), and free carrier dispersion (FCD). Thermo-optic effect (TOE) is particularly discussed in detail, since

this work based on thermo-optic effect (TOE) due to the low frequency pump. And finally the thermo-optic study of silica and silicon resonators in the literature is discussed.

Chapter 3 starts with the introduction of optical WGM and the potential in photonics. The theory of WGM resonators is discussed with the Mie scattering theory, and then the spectral properties of WGMs are discussed. These properties include the quality factor, and the mode spacing. Finally, the techniques for coupling light to a microresonator are discussed.

Chapter 4 discusses the proposed work "Optical tuning of the WGM's of a Silicon Microsphere". The experimental setup is first discussed, an outline of the proposed experiments is given and then experiments with pump excitation in continuous wave (CW) and pulsed mode are discussed. Each of the pump excitation case for tuning the refractive index of silicon is separately discussed. And finally the observed resonance shift cases are summarized in a table.

Chapter 5 concludes the work and discusses the possible future work within the scope of this experiment.

Chapter 2

OPTICAL EFFECTS IN SILICON

In this chapter, optical effects in silicon are discussed. The refractive index change in silicon can be modified by optical pump or electrical pump signals. In fact these excitations are not the only means of changing the refractive index. For instance by pressure one can induce a refractive index change. The effects, which are discussed are the following, one photon absorption (OPA), two photon absorption (TPA), optical Kerr effect (TPA), charge carrier effects, free carrier absorption (FCA), free carrier dispersion (FCD), and thermo-optic effect (TOE). All the effects are discussed one by one and particular detailed discussion is dedicated to the thermo-optic effect (TOE), which is the effect of subject. The physical model for describing the thermo-optic effect (TOE) is given, and finally literature study based on the thermo-optic effect (TOE) is discussed.

2.1 Introduction

Silicon (Si) is transparent at wavelengths above 1.1 μm [24], and the high refractive index of Si provides tight optical confinement for optical waveguides. In this chapter, we will discuss the phase shifting mechanism of an electromagnetic wave in general and particularly silicon passive resonators by changing the refractive index of the microsphere. The refractive index of crystalline silicon can also be changed by the change in the charge carrier concentration ΔN by absorption (charge-carrier effects) or by an applied electric field E (Franz-Keldysh effect).

Changing the refractive index by absorption can lead to thermo-optic switching, or optical Kerr switching depending on the time regime with, which the refractive index is being modulated. For instance, the optical Kerr based switches need ultrafast change in the refractive index, since optical Kerr effect has very short response time (few fs), and require high pump power (few Watts) for switching [25] [26]. Thermo-optic switching, requires a response time in the ms regime and a response time of around 10 ms has been reported [27] in doped fibers, where the switching of the signal required powers of few mW's of power. Along these two effects, other processes, which occur because of absorption are free carrier absorption (FCA), two photon absorption (TPA), and free carrier dispersion (FCD). In fact, two photon absorption (TPA) leads to free carrier absorption (FCA) and free carrier dispersion (FCD).

Electrically changing the refractive index of a material is called electro-optic modulation. In response to the applied electric voltage, the change in the real part of the refractive leads to electrorefraction, and a change in the imaginary part of the refractive index leads to electroabsorption. The electrooptic effects have been well studied and demonstrated in silicon. Ultrafast electrooptic modulation in a Si slot waveguide with silicon organic hybrid (SOH) approach instead of plasma effect modulators has been demonstrated [28]. This approach leads to strong modulating fields even for very small voltages and provides high modulation efficiencies. The performed work has 42.7 Gbits/s of rate with an increased modulation and low optical loss. An integrated silicon modulator at an operating frequency more than 100 GHz using SOH approach has been demonstrated [29]. Further, electrooptic modulation in a silicon on insulator (SOI) waveguide exhibiting a modulation depth of 80% for a DC power consumption of as low as 14 μW has been demonstrated [30]. Electrooptic modulation capable of high speed modulation with a bandwidth beyond 20 GHz in a Mach-Zehnder silicon waveguide is also

shown [31]. However, the functionality of these electrooptic modulators still requires an electrical pump signal.

The main advantage of using thermooptic switching is polarization insensitive operation and switching speeds on the order of milliseconds [32]. Knowing the thermooptic effect of an optoelectronic system is important for correcting the malfunctioning of the devices, such as distributed feedback (DFB) lasers, optical couplers, and waveguides. Thermooptic switches in silica and polymers are already commercially available.

2.2 One photon absorption in bulk silicon

One photon absorption (OPA) is a linear optical process, in which a photon has energy (more than the bandgap energy) to excite a carrier from the valence band to conduction band. In this study, the pump laser photon energy is 3.06 eV, which makes OPA the effect of subject.

2.3 Two photon absorption in bulk silicon

Two photon absorption (TPA), is a nonlinear optical process, where two photons are simultaneously absorbed to excite the carriers to higher energy levels in the conduction band from valence band [33]. TPA depends on the optical absorption and the refractive index. In Fig. 2.1, it is shown that, when the combined energy of the incident two photons is greater than the bandgap energy of silicon (E_g = 1.12 eV), then they will be absorbed, and will excite an electron from the valence band to the conduction band. The degenerate TPA is the case, when two photons of same wavelength (λ_1 in figure 2.1) are absorbed. In the non-degenerate TPA, instead of two identical photons, one incident photon at a certain wavelength (λ_1 in the Fig. 2.1) is absorbed together with another photon at a different wavelength (λ_2 in the figure), leads to TPA.

The non-degenerate TPA might be stronger than the degenerate TPA and is polarization dependent [33].

TPA process leads to the generation of free carriers. The density of free carriers depend on the incident pump intensity. The generated free carriers lead to free carrier absorption (FCA) and free carrier dispersion (FCD) in silicon. Normally FCA and FCD induced by TPA are performance degradation parameters for an optical system. However the knowledge of TPA and TPA induced FCA and FCD have applications in autocorrelations for pulse degradation [34], fluorescence microscopy [35], and all optical switching [36].

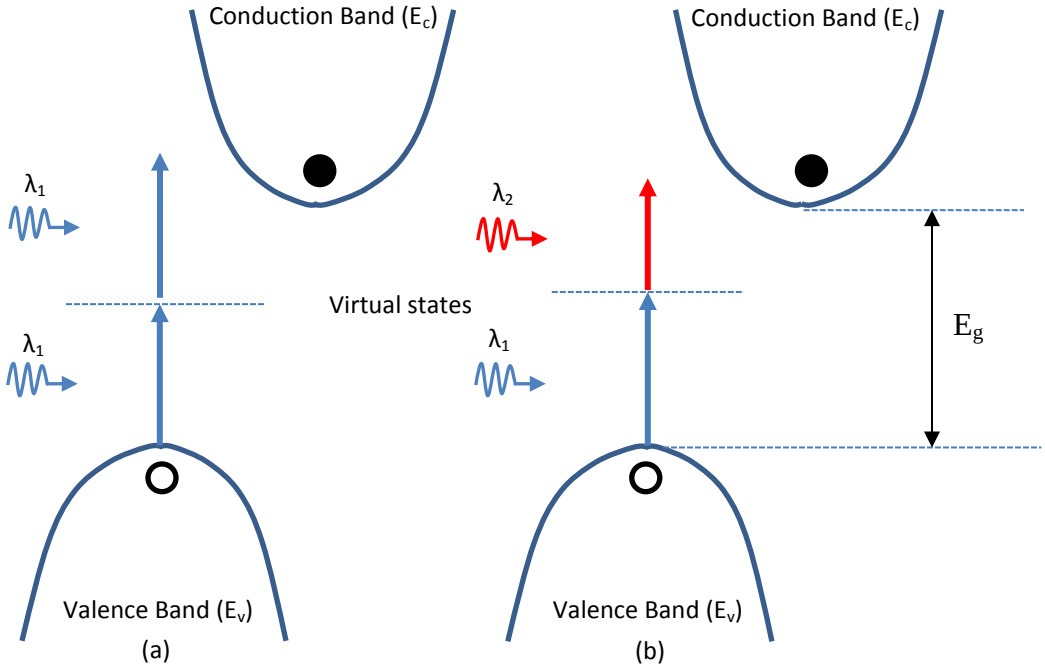

Figure 2.1. (a) Degenerate and (b) non-degenerate TPA in silicon.

2.4 Optical Kerr effect in bulk silicon

Optical Kerr effect describes the change in refractive index of a material in response to the intensity of light that propagates through the optical material. This definition is strictly for the optical Kerr effect, while there exist electro-optic Kerr effect (DC Kerr effect), which occurs in a material in response to the applied electrical pump. Kerr effect is different than the Pockels' effect in a way that, in Kerr effect the change in the refractive index is proportional to the square of the electric field of the pump, and not linearly proportional, which is the case in Pockels' effect.

When an intense beam of light passes through a material, a nonlinear polarization is generated, which in turn modifies the propagation of the light beam. Kerr effect is a third order nonlinear effect and for a given optical system nonlinearity can be written as:

$$P(t) = \varepsilon_0(\chi^1.E(t) + \chi^2.E(t)E(t) + \chi^3.E(t)E(t)E(t) + \cdots) \quad (2.1).$$

In previous Equation, $\chi^3.E(t)E(t)E(t)$ corresponds to optical Kerr effect, and is strong in silicon. Since silicon is a centrosymmetric crystal, lacks inversion symmetry, and doesn't possess the even power nonlinear effects, e.g., $\chi^2.E(t)E(t)$ [37]. The change in the refractive index can occur until extremely high power optical powers after which, the Kerr effect saturates [38].

2.5 Charge-carrier effects in bulk silicon

The optical properties of silicon are affected due to absorption. Because of absorption following carrier effects are important: (1) free carrier absorption, (2) Burstein-Moss band filling, and (3)

Coulombic effects. All of these three effects act at the same time, but among them, Coulombic effect is the strongest [39]. Burstein-Moss band filling is an effect, where the apparent bandgap of a semiconductor material is increased. Burstein-Moss band filling happens due to the degenerate doping in semiconductors (Fig. 2.2). Degenerate doping in semiconductors occur, when the electron holes concentration exceeds the conduction band edge density of states. As the doping concentration is increased, electrons populate the energy bands in conduction band due to which, the Fermi level gets higher in energy, and lies in conduction band. Therefore as shown in the following Figure. Apparent bandgap = actual bandgap + Burstein-Moss shift

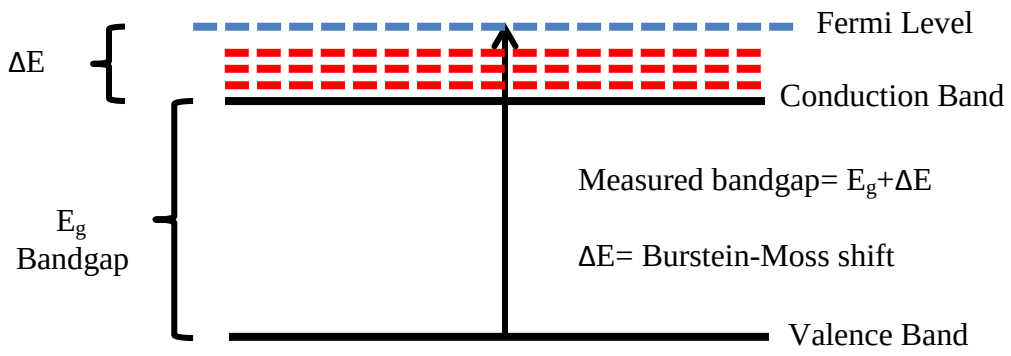

Figure 2.2. Burstein-Moss band filling effect.

The Fermi level gets higher in energy level, and a blue shift is observed due to Burstein-Moss band filling.

2.6 Free carrier absorption in bulk silicon

Free carrier absorption (FCA) is a process, where the photon energy is absorbed either in the conduction band or the valence band so FCA doesn't generate electron hole pairs, rather leads to intraband carrier transition and thus can produce heat [40]. FCA depends on the wavelength and the FCA coefficient linearly depends on the carrier concentration [41] [42], while some suggests a square root dependence [43] of the FCA on carrier concentration at room temperature. The free carrier absorption (FCA) of a semiconductor is given by:

$$\alpha_{FC} = \left(\frac{e^3\lambda^2}{4\pi^2 c^3 \epsilon_0 \mathrm{N}_{mat}}\right)[\Delta N_e/m_{ce}^*\mu_e + \Delta N_h/m_{ch}^*\mu_h] \qquad (2.2)$$

where e is the electron charge, N_{mat} the refractive index of the material, m_{ce}^* the effective mass of electrons, and m_{ch}^* the effective mass of holes, μ_e the electron mobility, μ_h the hole mobility, ΔN_econcentration of electrons, and $\Delta N_h$and concentration of holes.

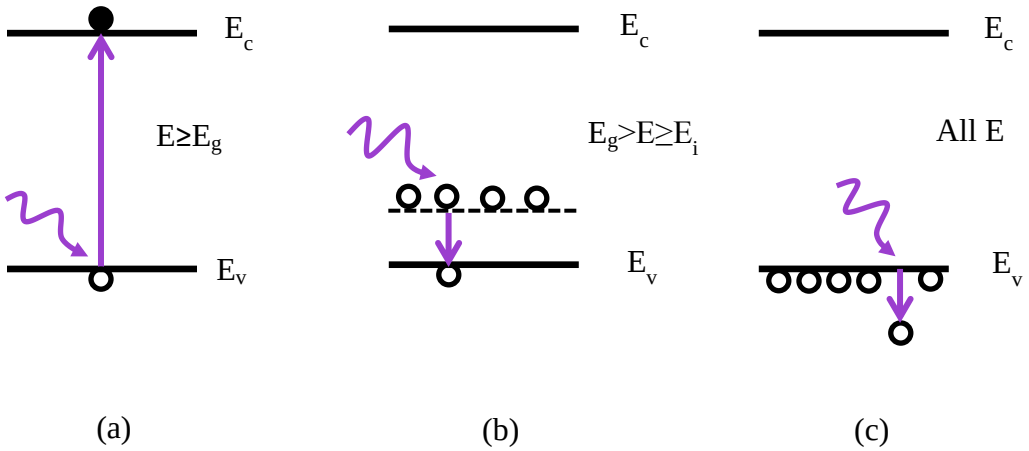

Figure 2.3. (a) Intrinsic, (b) extrinsic, and (c) FCA mechanisms in a p-type semiconductor.

Fig. 2.3 shows the case of a p-type semiconductor: (a) the intrinsic absorption in which, carrier gets absorbed from valence band into conduction band and this happens, when the incoming photon energy is higher than the bandgap energy, (b) extrinsic absorption, where the incoming photon energy is in between the intrinsic and extrinsic bandgap and (c) shows the intraband absorption or FCA, where the incoming photon is absorbed in either the valence band or conduction band.

2.7 Thermo-optic effect (TOE) in bulk silicon

The thermal modulation of the refractive index of a material is termed as thermooptic effect. Thermooptic effect (TOE) is described in terms of thermooptic coefficient dN/dT and the thermal expansion coefficient for a given material, however the thermo-optic coefficient, due to electronic and lattice effects, is more generally used to describe the phenomenon. The complex refractive index of a material can be written as:

$$\mathrm{N}\text{-}i\mathit{k} \tag{2.3},$$

where N is the conventional index (real part) and k is the optical extinction coefficient which is related to linear absorption coefficient ɑ by:

$$k = \frac{a\lambda}{4\pi} \tag{2.4}.$$

Kramers-Kronig analysis holds relationship between absorption k and refractive index n of a transparent medium [44] [45]. The relation also holds between Δk and ΔN. And the complex dielectric function can be written as:

$$\varepsilon = \varepsilon_1 - i\,\varepsilon_2 \tag{2.5}$$

N and ε are related by:

$$N^2 = \varepsilon \tag{2.6}$$

where ε_1 and ε_2 can be known from the knowledge of the real and imaginary part of the complex refractive index respectively.N, *k*, ε_1 and ε_2 are optical constant, which depend on the photon energy. So a change in ε, will cause a change in N.

The three mechanisms, which are making the temperature dependence of the dielectric constant of a material are: (1) a direct volume expansion effect, (2) the effect of volume expansion on the polarizability, and (3) the effect of the temperature on polarizability. All these effects combine to contribute to the temperature dependence of the dielectric function and at constant pressure is given by [46]:

$$\frac{1}{(\epsilon-1)(\epsilon+2)}\left(\frac{\partial\epsilon}{\partial T}\right)_P = -\frac{1}{3V}\left(\frac{\partial V}{\partial T}\right)_P + \frac{1}{3\alpha_m}\left(\frac{\partial\alpha_m}{\partial T}\right)_P\left(\frac{\partial V}{\partial T}\right)_P + \frac{1}{3\alpha_m}\left(\frac{\partial\alpha_m}{\partial T}\right)_P \tag{2.7}$$

The effect due to volume expansion is a decrease in the dielectric constant of the material due to enhancement of the interatomic spacing in the lattice with change in temperature. The polarizability of the material increases with both volume expansion and temperature.

The thermal expansion of ionic materials having low melting point is high and the thermooptic coefficient is negative for ionic materials. Similarly in polymers, the thermooptic coefficient is negative because of strong thermal expansion, which causes density change. For nonlinear crystals, having high melting points and strengths, the thermooptic coefficient is high compared

to thermal expansion coefficient, and the thermooptic coefficient is positive. The temperature dependent polarizability of a material is mostly positive, and this temperature dependent polarizability is important in defining the temperature dependence of the dielectric function of a material.

The dielectric susceptibility in transparent regime has electronic contribution and lattice contribution, which is written as [46]:

$$d\mathrm{N}/dT = (d\mathrm{N}/dT)_e + (d\mathrm{N}/dT)_l \tag{2.8}$$

The electronic contribution is due to the band to band transitions. Each of these contributions are individually written as:

$$(d\mathrm{N}/dT)_e = \frac{1}{2\mathrm{N}}\left[4\pi\chi_e\left(-3\alpha - \frac{2}{\omega_g}\frac{d\omega_g}{dT}\frac{1}{1-\omega^2/\omega_g^2}\right)\right] \tag{2.9}$$

$$(d\mathrm{N}/dT)_l = \frac{1}{2\mathrm{N}}\left[4\pi\chi_l\left(-3\alpha + \frac{2}{e^*}\frac{de^*}{dT} - \frac{2}{\omega_0}\frac{d\omega_0}{dT}\frac{1}{1-\omega^2/\omega_0^2}\right)\right] \tag{2.10}$$

where χ_e and χ_l are the electronic and lattice susceptibilities, respectively, ω_g the average bandgap energy, e^* the transverse effective charge, and ω_0 the phonon angular frequency.

There are two sorts of physical effects, which lead to thermooptic effect (TOE). The first is thermal expansion, where with an increase in temperature, material expands and becomes less dense, which reduces *n*. If this was the only effect to happen, then $(d\mathrm{N}/dT)$ would be negative.

However, there occurs another effect, in which the energy levels of the material change with temperature. This model suggests that, for semiconductors the electronic contribution is dominant, since the bandgap variation with temperature is higher than the variations of thermal expansion due to high melting points of the semiconductors. The temperature dependence of the thermooptic effect (TOE) has been studied [47], where the theoretical study based on single and double oscillatory model and experimental measurement have been presented to analyze the temperature dependent refractive index change for the temperature range of 300-600 K at 1.5 μm wavelength. Silicon has the highest thermooptic coefficient at 1.5 μm of wavelength:

$$\frac{\Delta \mathrm{N_{sph}}}{\Delta T} = 1.86 \times 10^{-4} K^{-1} \qquad (2.11).$$

The thermooptic coefficient of Si is two orders of magnitude stronger than the thermal expansion coefficient of Si, so the thermal expansion coefficient affects the WGMs two orders of magnitude weakly.

2.7.1 Thermo-optic wavelength tuning in resonators

When the material is illuminated with an optical pump the amount of shift in resonance corresponds to a change in the refractive index and can be calculated using:

$$\frac{\Delta \mathrm{N_{sph}}}{\mathrm{N_{sph}}} = \frac{\Delta \lambda}{\lambda} \qquad (2.12)$$

By knowing the amount of change in the refractive index, we can estimate the temperature required for the amount of shift in resonant wavelength observed using (2.11).

2.7.2 Thermo-optic effect (TOE) in silica waveguides and resonators

A fast (ns regime) thermooptic switching in a Cobalt doped fiber has been demonstrated by [48]. The purpose of doping with cobalt is again enhancing the absorption. In this work, a short 2 m length of optical fiber was spliced in a Sagnac loop and the purpose of the loop is to provide switching much faster than the relaxation time of the fiber material. The thermal change in the refractive index was carried with 25 ns pulse at 720 nm, while the source wavelength was 830 nm. The analysis has shown 7 ns and 46 ns of switching durations in a 2 m and 10 m fiber lengths, respectively.

The thermooptic effect on the WGMs of a glass microsphere has been demonstrated [49]. The work was carried out with a glass microsphere of 30 µm, which was placed in an electric furnace to provide a temperature change from room temperature to 950 K. This results in a red shift 10 pm/K.

Thermooptic switching in a glass microsphere of size 250 µm coated with a polymer (DOO–PPV) poly(2,5-dioctyloxy–1,4-phenylenevinylene) has also been demonstrated [50], again the purpose of coating the microsphere with an absorbing polymer was to enhance the absorption. In this work, 405 nm laser was employed to thermally change the refractive index of the microsphere. The microsphere was excited for its WGMs at 1.55 µm by evanescent coupling and in response to modulation of the sphere, WGM shifts as large as 3.2 GHz were observed. This shift was achieved with a pump intensity of ~10^4 mW/cm^2.

2.7.3 Thermo-optic effect in SOI sphere

The thermooptic effect (TOE) has been realized [51] in a silicon coated silica microsphere of size 150 µm. The microsphere was excited for it WGMs with a 1450 nm tunable laser and to thermally modulate the refractive index of the silica 488 nm laser was employed. Here in this work the reason for coating the sphere with silicon is to enhance the absorption for strong TOE. The work suggested power as low as 3 µW was sufficient to shift the WGM by half a linewidth of the resonance, which means full switching (resonance shift by 2 linewidths) would require at least 6 µW of power.

2.7.4 Thermo-optic effect (TOE) in silicon resonators

The thermal bistability in a silicon microdisk of 4.5 µm radius and 340 nm of thickness has been demonstrated [52]. In the phenomenon of thermal bistability, because of the absorbed power in the resonator, heat is produced, which causes a red shift in the transmission. The model of this work is as follows: the input power at 1454 nm corresponds to an intensity of 500 MW/cm^2 and this much intensity leads to effects such as two photon absorption (TPA) generated free carriers and the generated free carriers produces free carrier dispersion (FCD), and overall these effects produce heat. Overall thermal bistability has been observed with powers as low as 35 µW.

Chapter 3

WHISPERING GALLERY MODE (WGM) RESONATORS

This chapter discusses the optical resonances i.e., whispering gallery modes (WGMs) in a microspherical resonator. In section 3.1 an introduction is given the origin of the WGM and the potential of WGM, which has already been exploited in light based technologies.

In terms of Snell's law, light at the boundary between two media leads to the excitation of the WGM. When the wavelength of interest is comparable or smaller than the resonator size, Mie scattering becomes dominant for describing the behavior of the light-matter interaction. And Mie theory is discussed in section 3.2 by defining the size parameter and then in terms of size parameter the resonance condition is given. In section 3.3 the spectral properties of WGM are discussed, which includes quality factor and mode spacing. And finally the different available techniques for coupling light to resonator are discussed in section 3.4, which includes prism coupling, optical fiber half coupler use, tapered fiber coupling, and planar waveguide coupling. Particular discussion is about optical fiber half coupler (OFHC), which is used in this work.

3.1 Introduction

Light matter interaction has already paved the path for 21st century technology development and like 20th century was century of electronics, the 21st century is predicted as the century of photonics. Optical resonators [53] [54] are building blocks for the realization of optical systems. Particularly WGMs have been studied well, since the work [55] published by Lord Rayleigh in

1910-12, who studied the WGMs and provided the correct attributes for the first time, when he observed the phenomenon of listening to the audible whisper running around the interior of the dome of St. Paul's Cathedral in London at any point of the wall of dome [56]. He attributed this phenomenon as the surface focusing of the sound waves traveling along the wall surface of the dome. Based on this observation, he suggested the existence of WGMs for electromagnetic waves.

WGMs exhibiting small mode volumes, high power densities, and narrow linewidths, have been studied for optical systems with different resonator structures like cylindrical toroid geometries, micrometer sized droplets, and spheres [56] [57]. So WGMs are not only supported by spherical resonators but toroidal, cylindrical and disk structures also support WGMs. Applications like an optical add drop filter [58], biomedical sensing [59], thermooptical switching [60], broadband light management for high throughput ultrathin film absorbers [61], photonic crystal cavities [62] [63] have been realized experimentally with WGM resonators. Also electrically tuning the refractive index of a silicon microsphere for shifting the resonance has been observed [64]. WGMs are very sensitive to small refractive index or shape changes in the structure of the resonator [65] and thus possess significant interest for optical communication application. Thus WGM resonators can be used towards the realization of all optical functional devices.

WGM resonances are formed in a cavity, when an electromagnetic wave, which is totally internally reflected, starts circulating, and is confined by the cavity surface. The electromagnetic wave, while trapped in cavity makes surface oscillations. As the optical resonance in a WGM is a function of the resonator morphology, they are also morphology dependent resonances (MDRs), since morphology means dependence on the shape of the resonator.

A light mode in a spherical resonator is defined by the mode numbers *l*, *n*, and *m*, where *l* represents the field distribution in the radial direction, *n* represents the field distribution in the polar angular direction, and *m* represents the field distribution in the azimuthal angular direction.

Light at the interface between two boundaries can be explained by Snell's law given by equation:

$$\mathrm{N}_1 \sin\theta_1 = \mathrm{N}_2 \sin\theta_2 \qquad (3.1),$$

where N_1 is the refractive index of the incident medium and N_2 is the transmitted medium. When light traveling from N_1 into N_2, it can reflect and refract depending on the incidence angle and the polarization of the light field. There occurs an angle $\theta_c = \tan^{-1}\frac{\mathrm{N}_2}{\mathrm{N}_1}$ where total internal reflection (TIR) occurs and due to the symmetry of the spherical geometry all the subsequent angles are the same and light gets trapped inside the sphere. Due to TIR, when the light wave enters the sphere only for the wavelengths, which corresponds to the resonance condition, microsphere acts as optical resonator. In WGMs light propagates by repeated TIR, while satisfying proper phase condition along the surface of the microsphere. The evanescent field of light travels in the cladding and has intensity profile which decays exponentially [66] and possess different optical properties at the interface between two media. In terms of TIR, the evanescent waves cannot be completely described but the explanation comes from the solution of the Maxwell's equation. Evanescent field waves are suitable for applications like sensing or detection of molecules, proteins with optical resonators [67].

3.2 Lorenz Mie theory for light scattering from a microsphere

Lorenz Mie theory describes the scattering of electromagnetic wave from spherical objects, where the size of the resonator is comparable to the wavelength [68] [69] [70]. The Mie theory details the light behavior and interaction with the resonator, i.e., the electric and magnetic field distribution inside and outside of the spherical resonator, and accounts for the amount of light being scattered.

The objects, which are smaller in size than the wavelength of the light, are described by Rayleigh scattering [71], a phenomenon, which describes the reason for the blue color of the sky.

The scattering of a spherical resonator in terms of Mie theory can be described, if we know the refractive index and the size of the resonator along with the refractive index of the medium around the resonator. The most important parameter in the Mie theory is the size parameter, which describes the light interaction inside and outside of the resonator:

$$x = ka \tag{3.2},$$

where k is the wave number and a the radius of the resonator. In order to find the lower and upper limit on the size parameter, we need to know the polar mode number *n* for the same lowest order radial mode number *l* and then, the inequality can be written as:

$$\frac{n}{\mathrm{N_{sph}}} \leq x \leq n \tag{3.3}.$$

The low order resonances are narrow in linewidths, while the higher order resonances have larger linewidths. In terms of size parameter, the resonance condition can be defined as:

$$x \leq n \leq x\mathrm{N_{sph}} \tag{3.4}.$$

And the Q factor can be defined as:

$$Q = \frac{\omega_\alpha}{\Delta\omega_\alpha} = \omega_\alpha \tau \tag{3.5},$$

Where ω_α is the resonance frequency, and τ the photon lifetime in the resonator.

Theoretically and experimentally the interest have been in low order resonances in response to elastic light scattering from spherical resonators, [72] [73] because of narrow linewidths of the resonances, unlike for high order resonances, for which linewidths are larger. The narrow linewidth feature is promising for nonlinear optics, where the processes grow with exp($g\tau$), where g is the gain of the process, and is the cavity storage time of the photon [72].

The internal intensity distribution of the incident wave at the interface between a dielectric waveguide and spherical resonator is determined by expanding the electric and magnetic fields of the incident wave in terms of spherical harmonic functions with appropriate boundary conditions. The expansion coefficients are $\mathrm{a_n}$ and $\mathrm{b_n}$, given below:

$$a_n = \frac{j_n(x)[N_\gamma x\, j_n(N_\gamma x)]' - N_\gamma^2 j_n(N_\gamma x)[x\, j_n(x)]'}{h_n^{(2)}(x)[N_\gamma x\, j_n(N_\gamma x)]' - N_\gamma^2 j_n(N_\gamma x)[x h_n^{(2)}(x)]'} \quad (3.6),$$

$$b_n = \frac{j_n(x)[N_\gamma x\, j_n(N_\gamma x)]' - j_n(N_\gamma x)[x\, j_n(x)]'}{h_n^{(2)}(x)[N_\gamma x\, j_n(N_\gamma x)]' - j_n(N_\gamma x)[x h_n^{(2)}(x)]'} \quad (3.7),$$

where $j_n(x)$ is the spherical Bessel function, $h_n^{(2)}(x)$ the second kind Hankel function, x the size parameter, $N_\gamma = N_{sph}/N_o$ the relative refractive index of the resonator, and the prime symbol shows the derivative of the argument with respect to the size parameter in the brackets.

3.3 Spectral properties of WGM resonance

Quality factor: The Q factor determines the photon lifetime in the resonator, which is a measure of the sensitivity of the resonator. The quality factor of a resonator has applications in nonlinear optics and quantum optics, where high Q is desirable. Applications like luminescence emission enhancement inside a cavity require moderate Q factor, and in the case of cavity-based photovoltaic devices, an optimum value of Q exists that depends on the absorption coefficient for achieving the maximum absorption efficiency [74]. The quality factor Q of a resonator is determined by many factors:

$$\frac{1}{Q} = \frac{1}{Q_{rad}} + \frac{1}{Q_{ss}} + \frac{1}{Q_{cont}} + \frac{1}{Q_{mat}} = \frac{\lambda_{FWHM}}{\lambda} \quad (3.8),$$

where for a given resonator Q_{rad}^{-1} is the radiative loss because of curvature, Q_{ss}^{-1} the surface scattering loss because of imperfections and scratches on the surface, Q_{cont}^{-1} the loss due to contamination on surface of resonator, and Q_{mat}^{-1} is material loss such as absorption. Among these losses, the Q_{rad}^{-1} vanishes, if the ratio between the resonator diameter and operating wavelength is greater than or equal to 15, i.e., $D/\lambda \geq 15$, where D is the diameter of resonator, and λ the operating wavelength. Q_{cont}^{-1} can be limited by making sure the fabrication of the resonator and experimental work place dust and contamination free, and Q_{mat}^{-1} by operating the resonator in the transparent region of operation. Q_{ss}^{-1} is estimated by Equation (3.9) using Rayleigh model for surface clusters comparable to molecular size.

$$Q_{ss} = \frac{\lambda^2 D}{2\pi^2 \sigma^2 B} \tag{3.9},$$

where σ and B are the rms size and the correlation length of surface inhomogeneities [75].

For a given resonator, when the refractive index contrast of the reflecting boundaries is high and the radius curvature of the resonator exceeds certain number of wavelengths, then the only factors, which can limit the Q, are material attenuation, and surface imperfections, because bending and radiative losses become negligible.

The optical loss of a resonator is an important parameter for its potential use, and WGM resonators exhibit low reflection and absorption losses, thus possess high quality-Q factors. The

highest Q reported, till date up to the best of our knowledge, is $Q>10^{11}$ in calcium fluoride resonator at room temperature, [76] and this Q is still limited by material impurity.

Mode Spacing: Light is trapped inside cavity by total internal reflection (TIR) and propagates along the surface. The propagation of the electromagnetic wave along the spherical path corresponds to scattering peaks for cases, in which the round trip optical path length is an integer multiple of incident wavelengths, which is the resonance condition, and given by:

$$m\lambda = 2\pi a \mathrm{N}_{\mathrm{sph}} \tag{3.10},$$

Equation (3.11) calculates the spacing between two adjacent polar modes of order n with same radial mode of order l:

$$\delta\lambda = \frac{\lambda^2}{2\pi a \mathrm{N}_{\mathrm{o}}} \frac{\tan^{-1}\sqrt{\mathrm{N}_{\mathrm{sph}}^2 - 1}}{\sqrt{\mathrm{N}_{\mathrm{sph}}^2 - 1}} \tag{3.11},$$

where λ is the resonant wavelength, a the radius of sphere, and $\mathrm{N}_{\mathrm{sph}}$ the refractive index of sphere. The mode spacing of WGMs can be thought in analogy with a Fabry-Perot resonator, [77] which represents the spacing between two consecutive polar modes of order *n* for the same radial mode of order *l*.

3.4 Resonator-waveguide coupling techniques

The techniques for coupling light to microspheres are optical fiber half coupler (OFHC) [78], tapered fiber coupler [79], planar waveguides [80], and prism coupler [81]. Among these techniques, prism coupling is the oldest used to couple light into waveguides. In this work, we have used a single mode OFHC for coupling evanescent Gaussian light beam to microsphere. OFHC is part of an optical fiber, which is polished near to the core of the optical fiber and buried in a glass block to expose the evanescent field of the light beam.

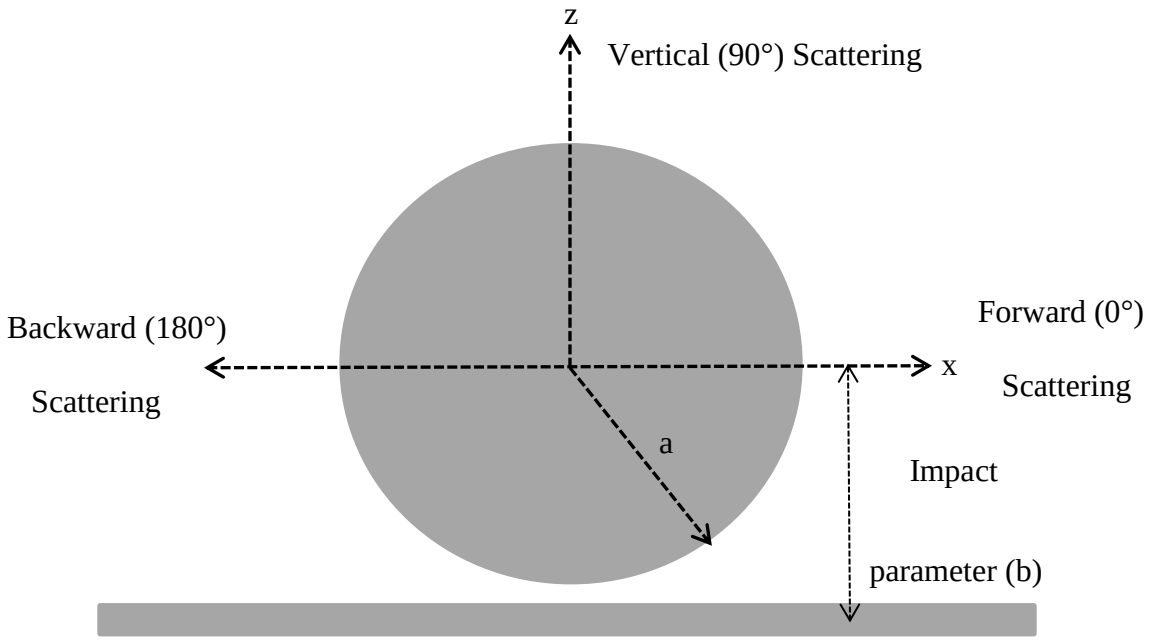

Figure 3.1. Silicon microsphere excitation by a single mode optical fiber half coupler (OFHC).

The microsphere is placed over the OFHC in order for the evanescent field of the optical fiber to interact with WGM of the sphere for energy exchange. The reason for choosing OFHC is, its small mode volume, which could lead to critical coupling [82] [83]. The number of modes, which can be carried over a coupler waveguide, is an important parameter for determining the efficient coupling of light to the microsphere. Single mode OFHC makes it easy by offering a single mode to be coupled to the microsphere.

The impact parameter, shown in Fig. 3.1, defines the distance between the Gaussian beam waist and the microsphere. The efficient excitation of the WGMs of a microsphere by a Gaussian beam, depends on the impact parameter. Choosing the right coupler determines the fate of the WGMs. Moreover along with an imperfection (dust and contamination) free OFHC, choosing the right impact parameter for the coupling is very critical.

Chapter 4

ALL-OPTICAL TUNING OF WGM'S OF A SILICON MICROSPHERE

In this chapter, WGM spectra of a silicon microsphere will be discussed. Afterwards the thermooptic shift in WGMs will be discussed. The proposed experimental work is divided into sections and each of the section is discussed in detail. Mainly the amount of shift in WGM is discussed in every case observed in response to the thermooptic effect (TOE), and based on that the change in refractive index is calculate and, an estimate is given for the required amount of temperature which corresponds well with the measured amount of temperature using the thermooptic coefficient of silicon. For all the proposed experiments the same experimental setup is used, and a slight modification for the experiments is performed for the neutral density filters, where a filter wheel is used to rotate the position of the filters for controlling the pump output. For every measurement, the pump beam is either focused or unfocused.

The thermooptic switching has been proposed and demonstrated in glass as material of interest and this is because of the optical fiber technology. This work is based on the ms regime optical tuning of the refractive index of a silicon microsphere of radius 500 μm. In the literature to the best of our knowledge, the thermo-optic study of a silicon microsphere has not been reported yet, so this work demonstrates the first ever experimental study of TOE of a silicon microsphere of radius 500 μm.

The reason behind experimental study of the TOE in silicon is to explore its potential for all optical switching and modulation, because (1) as discussed in section 1.1 the maturity of the

silicon material with standard CMOS industry, i.e., the fabrication and characterization techniques are quite mature and (2) the electrical and optical properties of silicon makes it potential candidate for bridging between electronics and photonics, and (3) the thermo-optic coefficient of silicon is three times higher than the other thermo-optic materials (for instance glass), and Si also possess high thermal conductivity, which is particularly important for the realization of fast thermo-optical systems [84]. The thermo-optic coefficient of silicon at 1.5 μm is $\Delta N_{sph}/\Delta T = 1.86 \times 10^{-4} K^{-1}$and thermal expansion coefficient is $2.6\times 10^{-6} K^{-1}$. This thermooptic coefficient is three times higher than that in glass [85], and it is two times more than that of $LiNbO_3$, which paves the path for Si devices such as thermo-optic switches, modulators, and sensors [86].

The extended transmission window, which silicon offers compared to silica, and the high refractive index, which provides tight mode confinement for the nonlinear effects [87] are another features of interest. Further, the excellent material properties, like high thermal conductivity, high optical damage threshold, and high third order nonlinearity, make silicon potential candidate for the realization of thermo-optic switching.

4.1 Experimental Setup

The experimental setup schematic is shown in Fig. 4.1. The temperature and laser current parameters of diode laser are controlled by a laser diode controller (LDC). The laser diode controller in turn is controlled by LabVIEW via general purpose interface bus (GPIB) IEEE-488 interface to a computer. The WGMs of the silicon sphere are excited with a tunable diode laser having a central wavelength at 1427 nm. An output power of 28 mW at 450 mA of laser current is delivered to optical fiber half coupler (OFHC) through a single mode fiber patch cord.

The OFHC is a single mode silica fiber buried in a glass block, and its surface scattering can be seen by a visual fault locator (VFL). A silicon sphere of radius 500 micron and refractive index of 3.5 is held top of the OFHC, and an x-y stage provides the adjustment mechanism for efficient coupling of the light to the microsphere. The electromagnetic wave is trapped inside the cavity by total internal reflection (TIR). Two InGaAs photodiodes (PD) are used, one for the 90° elastic light scattering and the second for the 0° transmission. The transmission through OFHC is connected to a Y-coupler, which is used to have simultaneous measurements of the 0° transmission through a PD and optical multimeter (OMM). The scattering and transmission signals are acquired in computer through a 100 MHz two channel digital storage oscilloscope (DSO) connected via GPIB. In order to avoid the pump detection in 90° scattering PD, a silicon wafer is installed.

We modulated the refractive index of the sphere with different intensities of pump laser both in continuous wave (CW) mode and pulse mode of operations. For pulse mode operation, we used an Agilent 33220A 20 MHz arbitrary waveform generator. For the case of CW mode operation, pump laser with average power of 10 mW and spot size of 1.76 mm is directed onto the sphere with unfocused beam and then the same operation but making the beam focused (spot size of 550 μm) with a converging lens of focal length 15 cm. Next, to see the thermal change in the refractive index, we used neutral density (ND) filters, which provide controlled output power for the pump laser in CW.

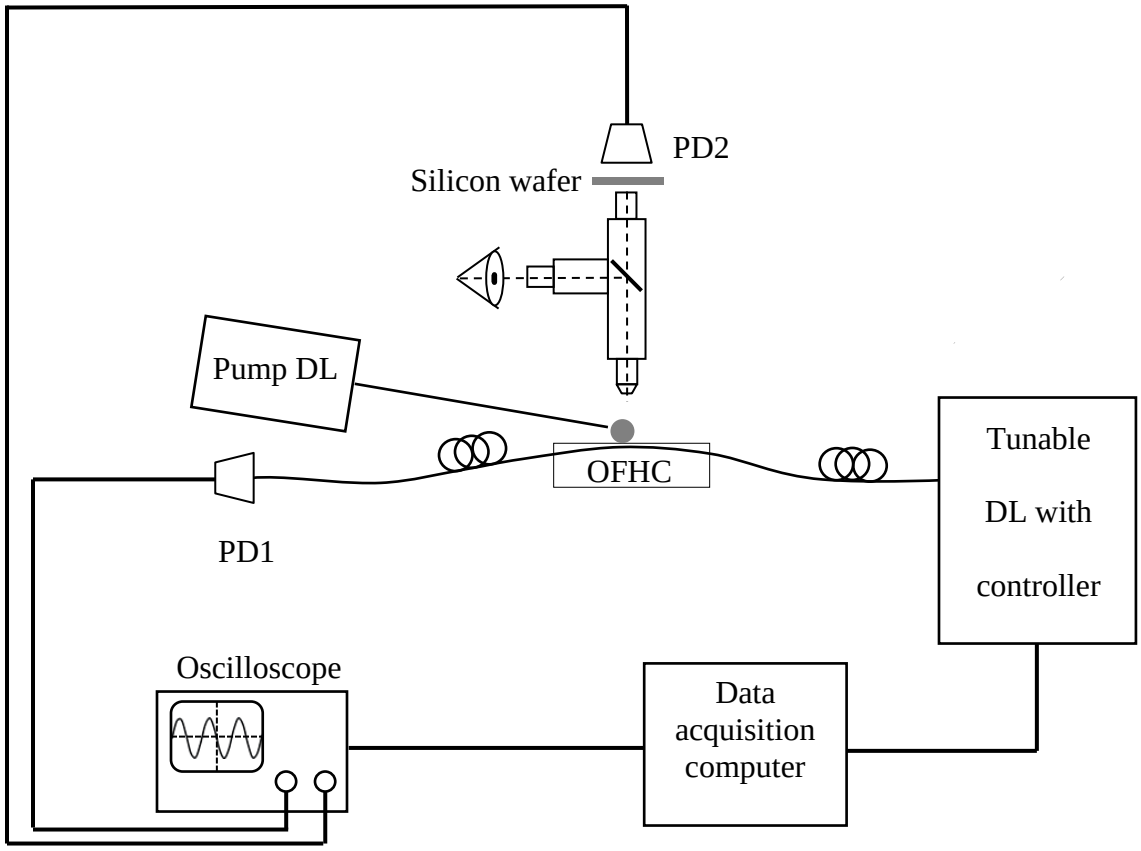

Figure 4.1: Experimental setup of all-optical tuning of scattering from a silicon microsphere.

To proceed with the work, we proposed to operate:

1) The pump laser in CW mode (full power) with unfocused beam
2) The pump laser in CW mode (full power) with focused beam
3) The pump laser in pulse mode with unfocused beam
4) The pump laser in pulse mode with focused beam
5) The pump power in CW mode (variable power) with unfocused beam
6) The pump power in CW mode (variable power) with focused beam

4.2 WGM of a silicon microsphere of radius 500 µm

Fig. 4.2 shows the WGM of a silicon microsphere, where the 0° is transmission (red curve) and 90° is scattering (blue curve) spectrum. The polar mode spacing observed is δλ = 0.23 nm, which corresponds well with the theoretical mode spacing calculation for a sphere of radius 500 µm by equation (3.11). The Q factor of resonance observed is 60000 calculated based on equation (6).

For this measurement the source laser is tuned from 1426.67 nm to 1427.607 nm by a temperature scan from 23.50 °C to 14 °C for a laser current of 450 mA. These parameters of the laser diode controller correspond to a wavelength window of 0.937 nm.

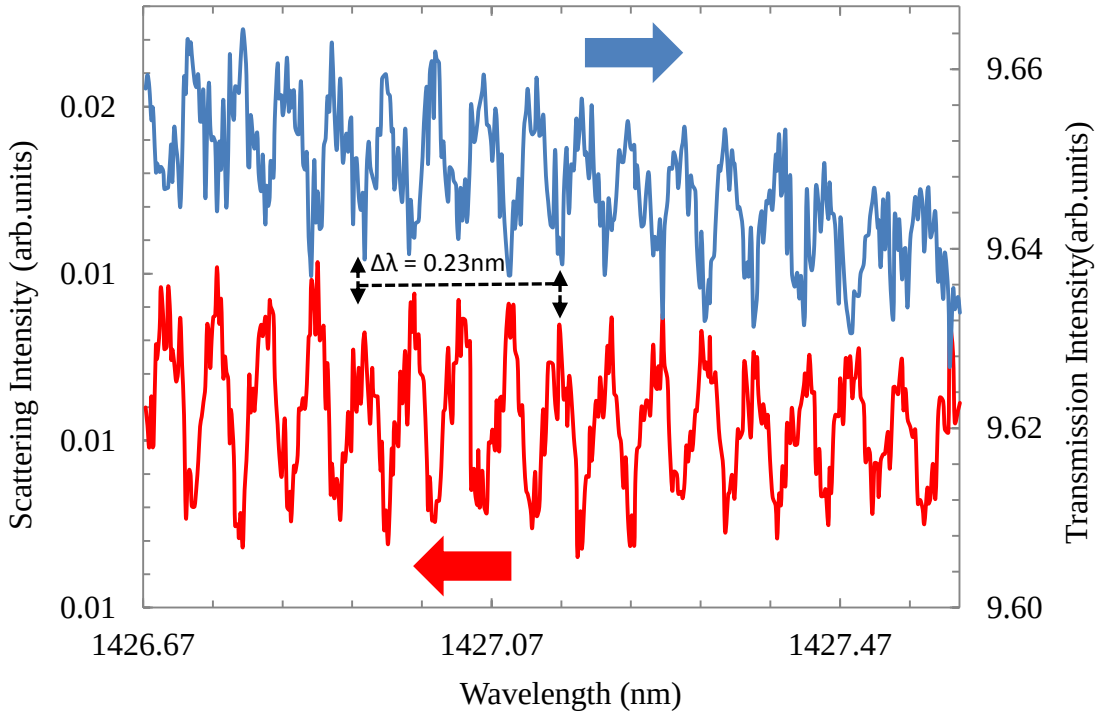

Figure 4.2. 90 ° scattering and 0 ° transmission of silicon microsphere.

First of all, in order to see the repeatability of resonances, we repeated the experiment five times and the resonances are appearing almost on the same position for a nonmodulated silicon sphere

shown in Fig. 4.3. For this measurement, the source laser is tuned from 1426.694 nm to 1427.606 nm by a temperature scan from 26 °C to 16 °C for a laser current of 450 mA. These parameters of the laser diode controller correspond to a wavelength window of 0.912 nm. The resonances correspond well with the theoretical mode spacing calculation and resonance positions. This measurement provide base for the expected resonance shift in response to modulation of the refractive index.

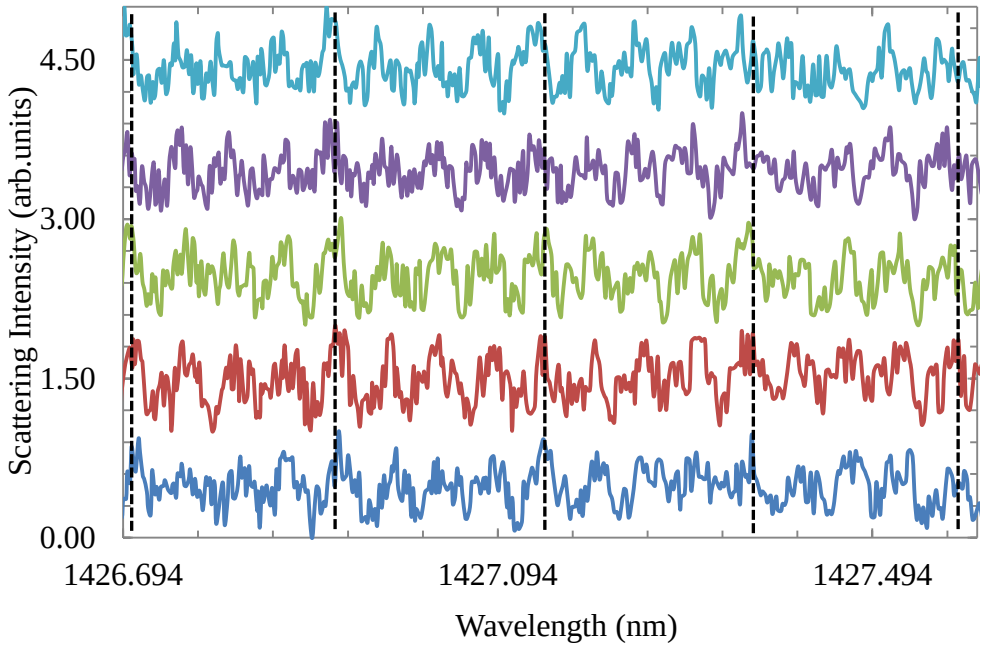

Figure 4.3: The repeatability of the resonances of a silicon microsphere.

The resonance condition given by Equation (3.10) changes in response to the modulation of the refractive index of the microsphere. When the refractive index of the sphere is modulated, resonances are red shifted. As discussed in chapter 2, the reason for the red shift of the resonance is the high thermooptic coefficient for silicon than the thermal expansion coefficient. Since the modulation of the microsphere is being done in millisecond (ms) regime, TOE is the dominant effect.

4.3 CW and pulsed pump excitation of the silicon microsphere

The pump laser is used in CW mode and pulse mode and all the proposed cases are discussed in detail one by one.

4.3.1 CW unfocused pump laser excitation

For this measurement, the probe laser is tuned from 1426.694 nm to 1427.606 nm by a temperature scan from 23.5 °C to 14 °C for a laser current of 450 mA. These parameters of the laser diode controller correspond to a wavelength window of 0.912 nm. Fig. 4.4 shows the change in the WGM spectra for the case of unfocused pump laser beam (spot size = 1.76 mm) where normalized transmission/scattering are plotted for 0% and 100% (bottom 2 spectra and top 2 spectra respectively) of modulation of the sphere. Here 0% is when pump laser is off and 100% is when pump laser is on in CW with output power 27.35 mW . The black dashed lines represent the dip and peak structure of WGMs of the sphere and the red dashed lines represent the shift in the WGM spectra. When the pump laser is turned on, WGMs of the sphere appeared to the right with respect to the non-modulated WGM of the sphere (0% spectra). The amount of shift in WGM observed in this case is 13.5 pm. Based on Equation (2.12), the calculated change in the refractive index for 13.5 pm of shift in the WGM is 3.29×10^{-5}. And the required temperature to make this much of change in the refractive index is 0.177 K estimated by using Equation (2.11).

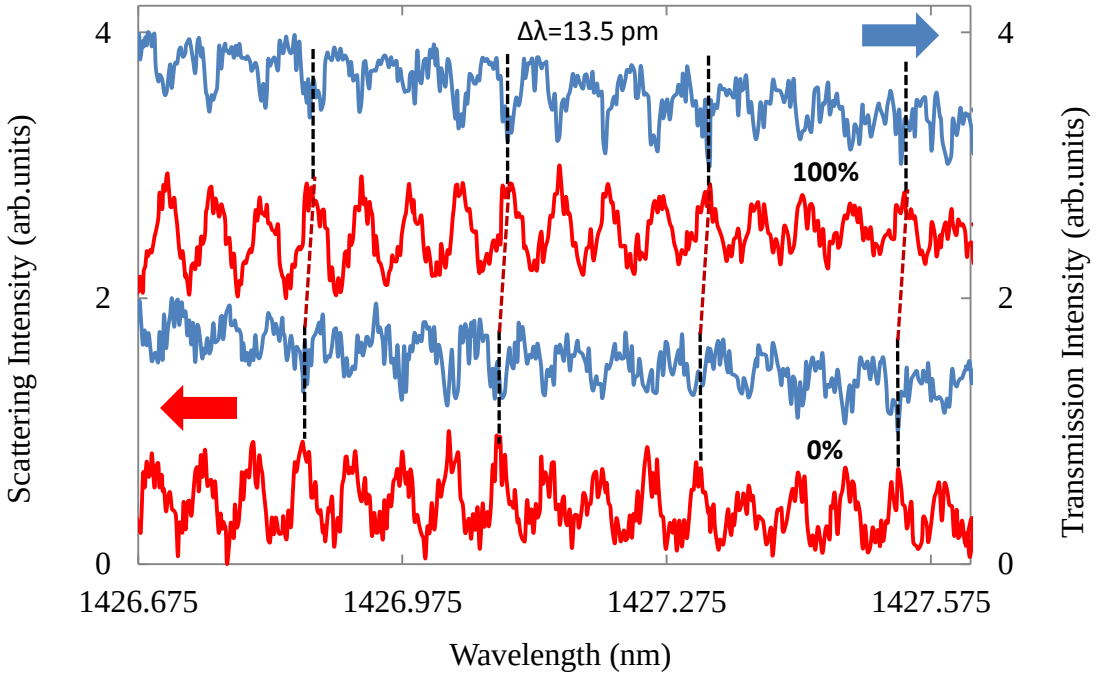

Figure 4.4: Unfocused CW 0% and 100% pump dependence of (a) transmission and (b) scattering.

4.3.2 CW focused pump laser excitation

For this measurement, the source laser is tuned from 1426.8622 nm to 1427.855 nm by a temperature scan from 26 °C to 16 °C for a laser current of 450 mA. These parameters of the laser diode controller correspond to a wavelength window of 0.9928 nm. Fig. 4.5 shows the change in the WGM spectra for the case of focused pump laser beam (spot size= 550 µm), where normalized transmission/scattering spectra is plotted for 0% and 100% (bottom 2 spectra and top 2 spectra respectively) of modulation of the sphere. Here 0% is, when pump laser is off and 100% is, when pump laser is on in CW mode with output power 22.45 mW. The black dashed lines represent the dip and peak structure of WGMs of the sphere and the red dashed lines

represent the shift in WGM spectra. When the pump laser is turned on, WGMs of the sphere appeared to the right with respect to the nonmodulated WGM of the sphere (0% spectra). The amount of shift in WGM observed in this case is 24.5 pm. The shift in the WGM observed for the focused and unfocused case shows more absorption in the case of a focused beam, since the beam spot of 550 µm is comparable to the 500 µm sphere radius. Based on Equation (2.12), the calculated change in the refractive index for 24.5 pm of shift in the WGM is 5.97×10^{-5}, the required temperature to make this change in the refractive index is 0.32 K estimated by using Equation (2.11).

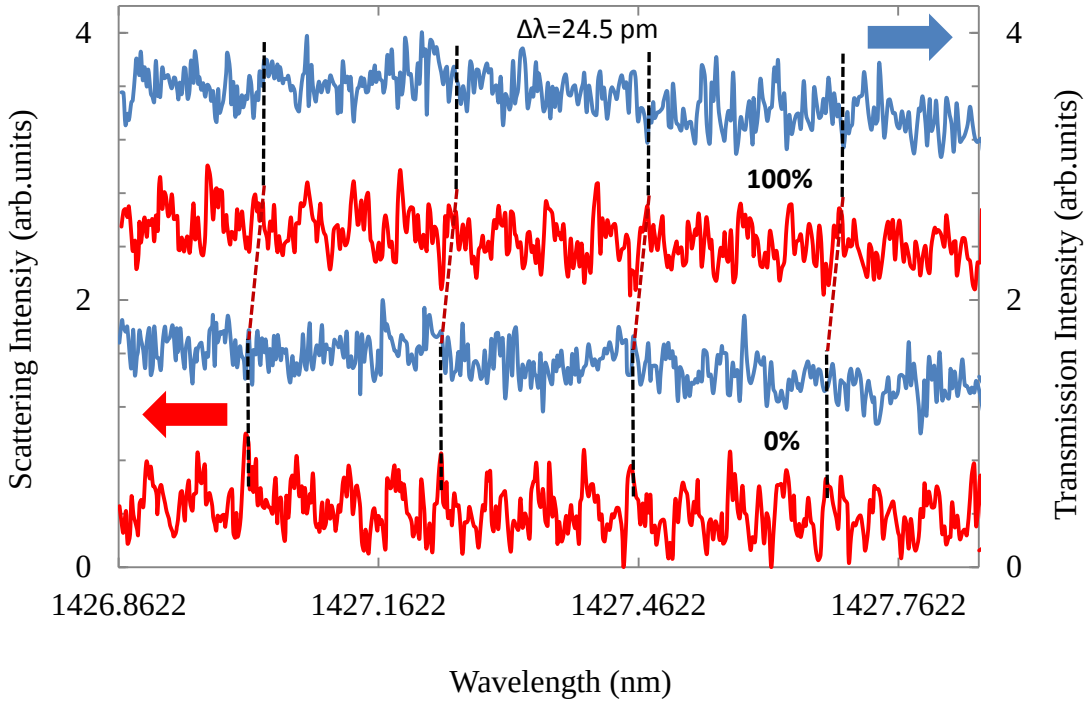

Figure 4.5: Focused CW 0% and 100% pump dependence of (a) transmission and (b) scattering.

4.3.3 Pump power measurement for different duty cycles of the pump laser

Next we used the pump laser in pulse mode and modulated the refractive index of the sphere at low frequency. For pulse mode operation, we used an Agilent 33220A 20 MHz arbitrary waveform generator. The pump power measurement for different duty cycles at 8 Hz is tabulated in Table 1, and the respective plot is shown in Fig. 4.6. The pump power measurement has been performed with Coherent Thermal Powermeter Power Max 5200 at Koç University Laser Research Laboratory.

Duty cycle	**Pump power**
%	mW
10	11.2
20	16.2
30	18.6
40	21.2
50	23.7
60	26
70	28.4
80	34.3
90	31.5

Table 4.1: Pump power measurements as a function of duty cycle.

From the plot of the pump power in Fig. 4.6, it is evident that at 8 Hz the maximum pump power is occurring at 80% duty cycle. The pump pulse excitation experiment is again done with pump beam unfocused and focused.

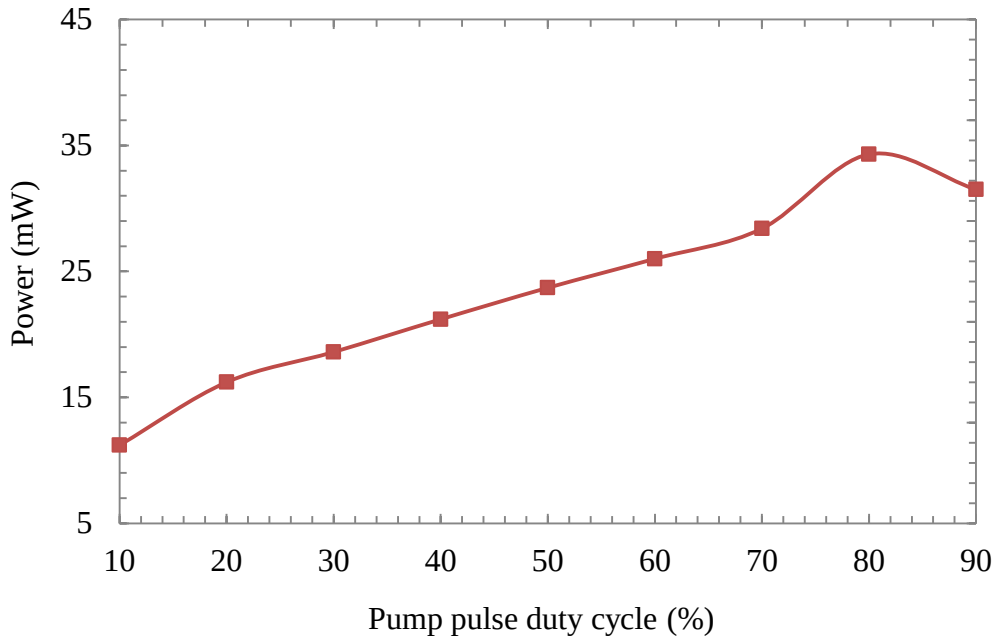

Figure 4.6: Pump power measurements as a function of the duty cycle.

4.3.4 Pulsed unfocused pump laser excitation

For this measurement, the source laser is tuned from 1426.675 nm to 1427.61 nm by a temperature scan from 23.5 °C to 14 °C for a laser current of 450 mA. These parameters of the probe laser diode controller correspond to a wavelength window of 0.935 nm. Figures 4.7a and 4.7b represent the transmission and scattering spectra for all the measurements from 0% to 100% of pump power (bottom to top), respectively. For the pulse mode pump excitation, the pump duty cycle is changed using a function generator from 10% to 90%, while the 0% is the nonmodulated WGM of the microsphere, and 100% is the WGM of the sphere, when the CW pump is on.

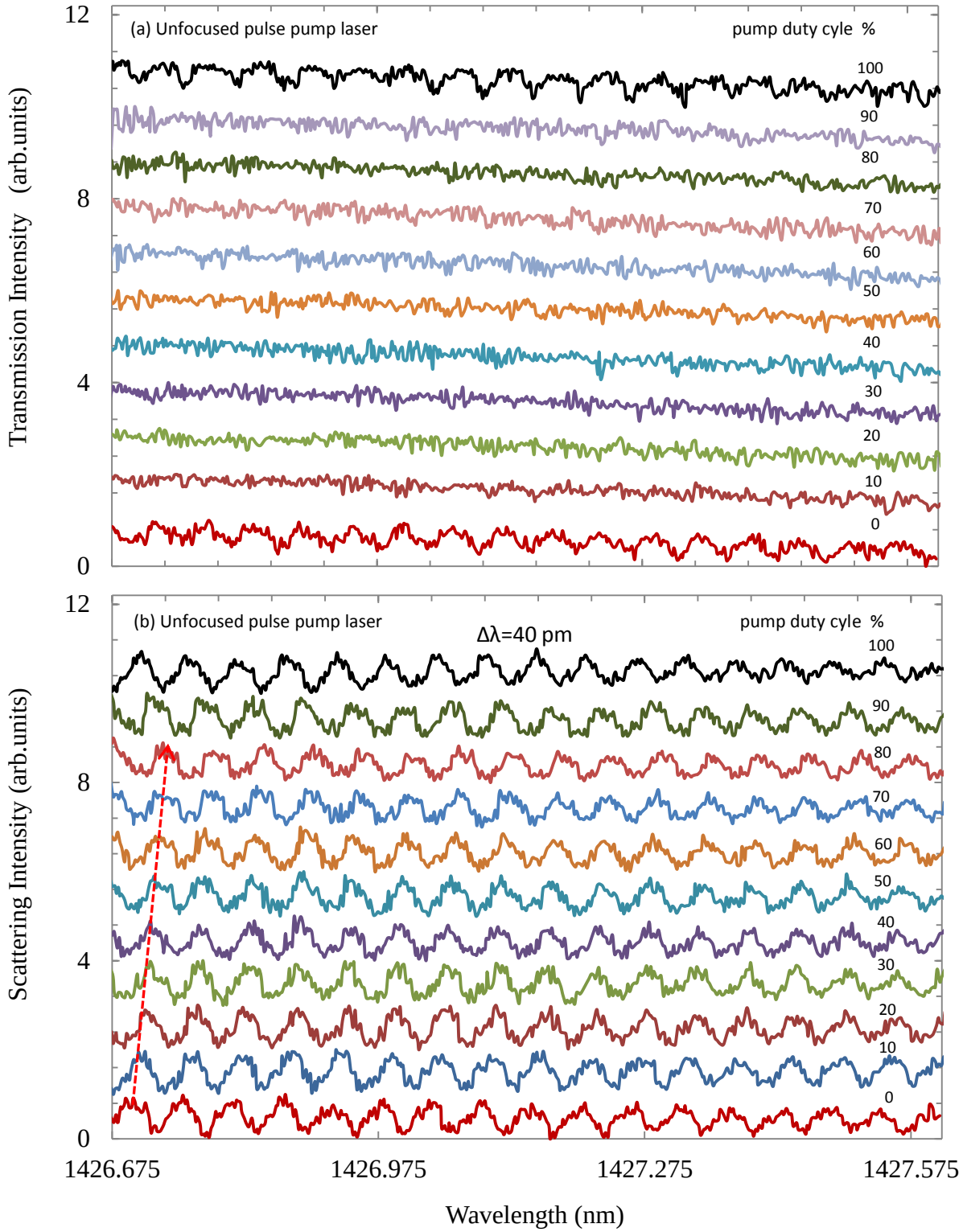

Figure 4.7: Unfocused pulse 0% - 100% pump dependence of (a) transmission and (b) scattering.

Every duty cycle correspond to different pump power, which is given in Table. 4.1. In the inset of the figures, the pump beam type and duty cycles are given. Here, the important observation is the shift in the WGM spectra of Fig. 4.7b, where the shift in WGM spectra is increasing with increasing pump power till 80% of duty cycle of the pump, where the maximum 40 pm shift is occurring. This observation is corresponding well with pump power measurement recorded in Fig. 4.6. Based on Equation (2.12), the calculated change in the refractive index for 40 pm shift in the WGM is 9.75×10^{-5}, and the required temperature to make this much of change in the refractive index is 0.52 K estimated by using Equation (2.11).

4.3.5 Pulsed focused pump laser excitation

For this measurement, the source laser is tuned from 1426.875 nm to 1427.85 nm by a temperature scan from 23.5 °C to 14 °C for a laser current of 450 mA. These parameters of the laser diode controller correspond to a wavelength window of 0.935 nm. Figures 4.8a and 4.8b represent the transmission and scattering spectra for all the measurements from 0% till 100% of pump power (bottom to top) respectively. For the pulse mode pump excitation, the pump duty cycle is changed using a function generator from 10% to 90%, while the 0% is the nonmodulated WGM of the microsphere and 100% is the WGM of the sphere, when the CW pump is on. In the inset of the figures the pump beam type and duty cycles are given. In this case, the WGM spectra for 0% and 100% of modulation are appearing resonant. For the case, when the pump is turned into pulse mode the WGM spectra are no more observable, and we are just observing the background signal. As can be seen from Fig. 4.8b, the WGM spectra of 0% and 100% are appearing resonant, also the WGM spectra for 90% duty cycle is recovering as this duty cycle is

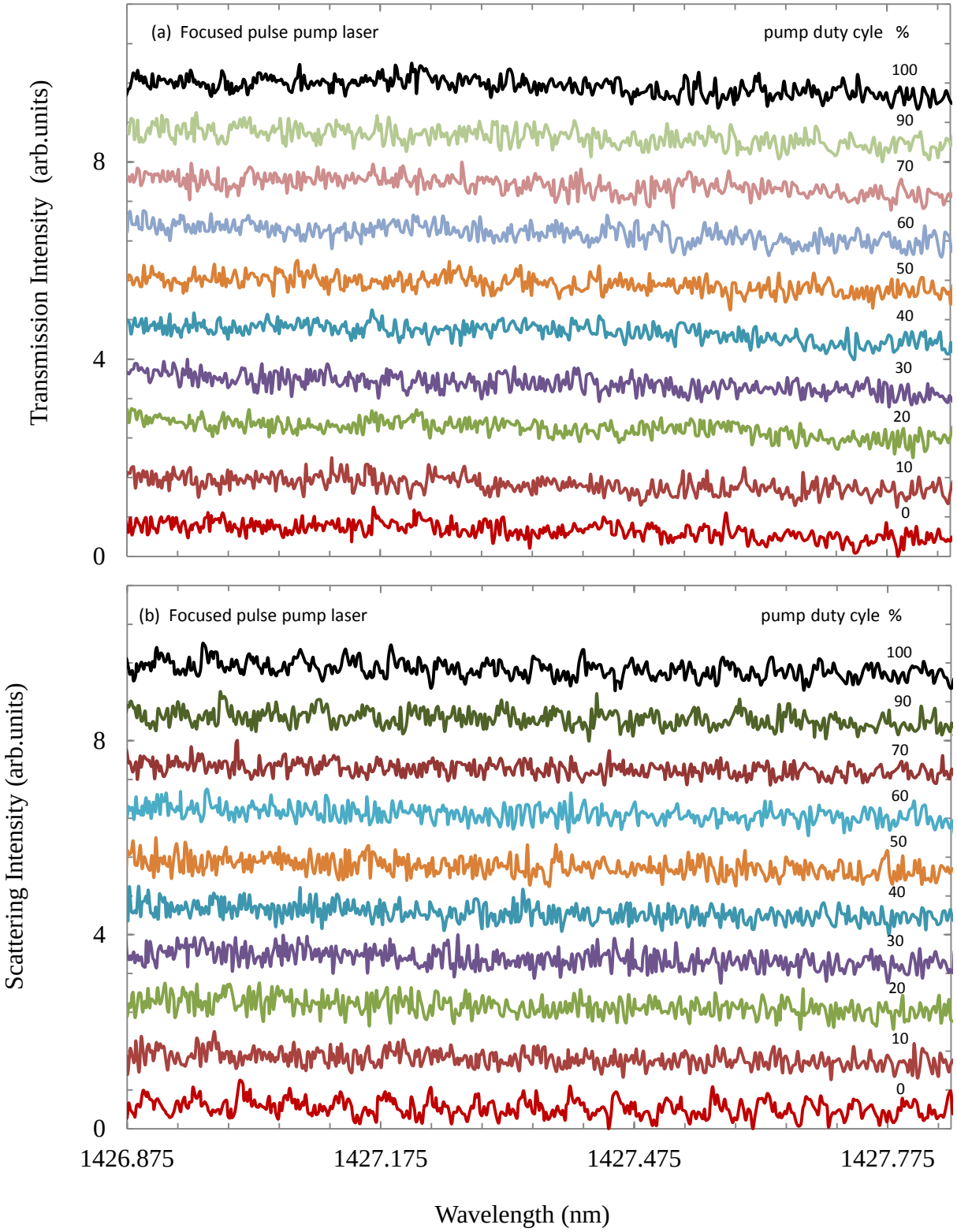

Figure 4.8: Focused pulse 0% - 100% pump dependence of (a) transmission and (b) scattering.

close to CW operation. For the pump duty cycles from 10% to 70% WGM spectra are no more observable. In the focused pulse case, the intensity, 15217 mW/cm^2 at 80% duty cycle, is considerably higher than the unfocused pulse intensity i.e., 1411.52 mW/cm^2 at 80% duty cycle, that the microsphere is off-equilibrium to observe any resonant peak. This observation is particularly important as it might be switching the input signal as has been observed by [51]. The behavior repeated with all the 9 measurements from 10% till 70% of pump duty cycle. And when the pump was tuned back to CW operation the WGM of the microsphere was appearing normal with resonant peaks in the spectra. Since for unfocused case, we saw that with increasing duty cycle of the pump, power is increasing until 70% here the WGM of the microsphere is recovering at 90% pump duty cycle.

4.4 CW intensity measurement of the pump laser

Towards proposed work, we changed the intensity of the pump laser by using neutral density (ND) filters in continuous wave mode. For this work, we used a filter wheel controlled by a LabVIEW program, which allows the selection of the desired ND filter. Again the work is done using pump laser with unfocused and focused beam. The transmission intensities with different ND filters are tabulated in Table 4.2. Neutral density (ND) filters are used in photonics to reduce the amount of light entering the lens and for a given ND filter the amount of optical power transmitted through it can be calculated by taking the logarithm of the ratio between incident power and the transmitted power, $\mathrm{ND} = -\log_{10}\frac{I}{I_0}$, where I is intensity after the lens and I_0 incident intensity.

Filter position in the wheel	Pump output
#	mW
2	0.020
1	1.17
3	2.93
5	4.44
6	6.39
4	9.45

Table 4.2. CW pump power measurements as a function of ND filters.

4.4.1 CW unfocused pump laser excitation with various intensities

For this measurement, the source laser is tuned from 1427.66 nm to 1428.67 nm by a temperature scan from 26.5 °C to 17 °C for a laser current of 450 mA. These parameters of the laser diode controller correspond to a wavelength window of 1.01 nm. Figures 4.9a and 4.9b represent the transmission and scattering spectra for all the measurements for different pump powers (bottom to top) respectively through 6 different ND filters, while the first bottom spectrum is the nonmodulated spectrum of the silicon microsphere. The inset of figures shows the pump mode and the amount of power for every measurement. It can be seen from the Fig 4.9b that, as the pump power is increasing a corresponding red shift of the WGM spectra is

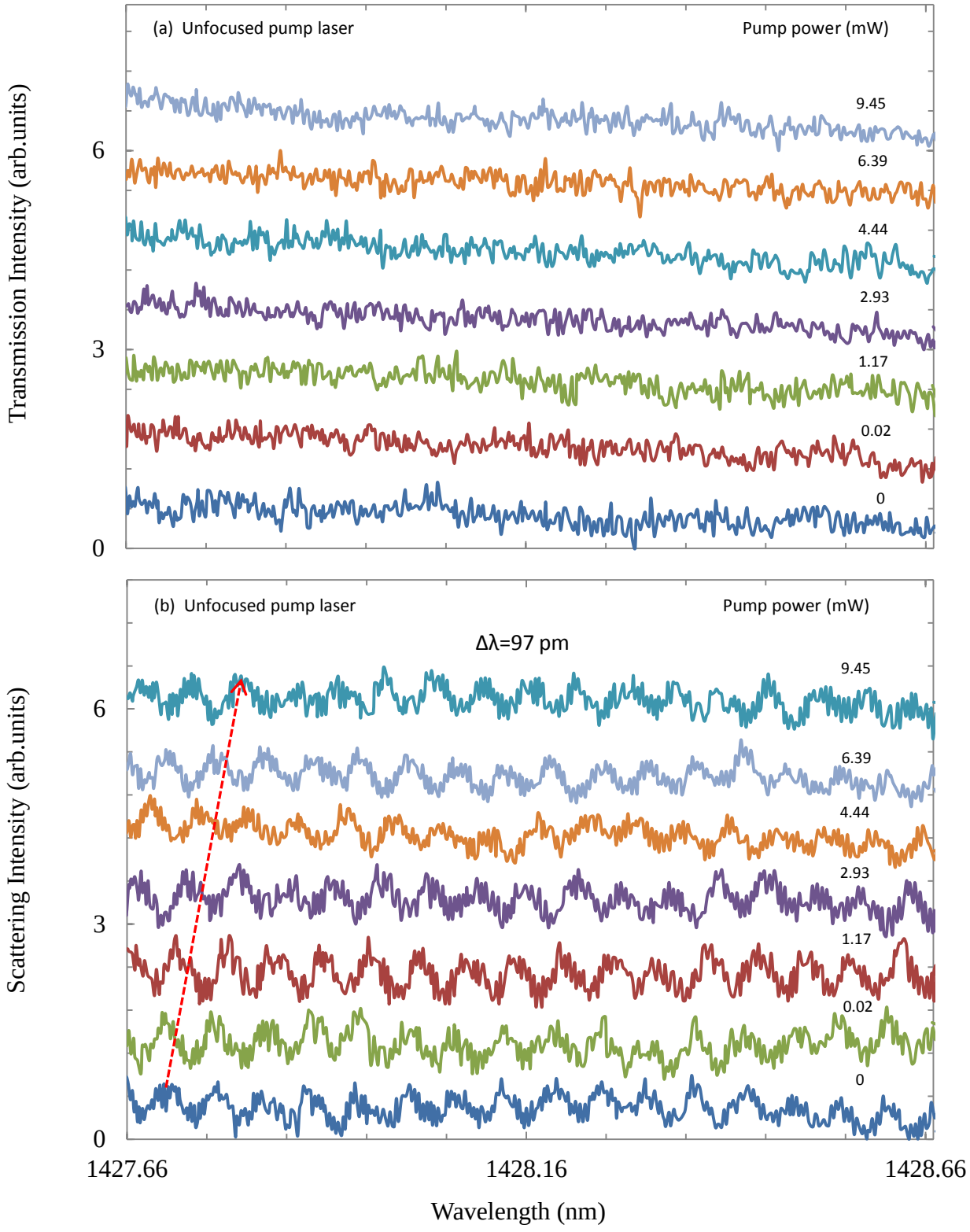

Figure 4.9: Unfocused CW pump intensity dependence of (a) transmission and (b) scattering.

observed. The shift is not linear (the dashed line is not linearly touching resonant peaks for all the measurements) as different ND filter offer different amount of transmissions as can be seen in Table. 4.2. The maximum shift of WGM is 94.6 pm shown by the red dashed arrow in starting from the non-modulated WGM of the sphere to the maximum pump power modulated WGM for this measurement. Based on Equation (2.12), the calculated change in the refractive index for 97 pm of shift in the WGM is 2.30×10^{-4}. And the required temperature to make this much of change in the refractive index is 1.24 K estimated by using Equation (2.11).

4.4.2 CW focused pump laser excitation with various intensities

For this measurement, the source laser is tuned from 1427.505 nm to 1428.502 nm by a temperature scan from 27 °C to 17 °C for a laser current of 450 mA. These parameters of the laser diode controller correspond to a wavelength window of 0.997 nm. Figures 4.10a and 4.10b represent the transmission and scattering spectra for all the measurements for different pump powers (bottom to top) respectively through 6 different ND filters, while the first bottom spectrum is the non-modulated spectrum of the silicon microsphere. The inset of figures shows the pump beam mode and the amount of power for every measurement. It can be seen from the Fig 4.10b that, as the pump power is increasing a corresponding red shift of the WGM spectrum is observed. The shift is not linear (the dashed line is not linearly touching resonant peaks for all the measurements) as different ND filter offer different amount of transmission as can be seen in Table 4.2. The maximum shift of the WGM is 273 pm, shown by the red dashed arrow in starting from the non-modulated WGM of the sphere to the maximum pump power modulated WGM for this measurement. Based on Equation (2.12), the calculated change in the refractive index for 278 pm of shift in the WGM is 6.66×10^{-4}. And the required temperature to make this much of change in the refractive index is 3.58 K estimated by using Equation (2.11).

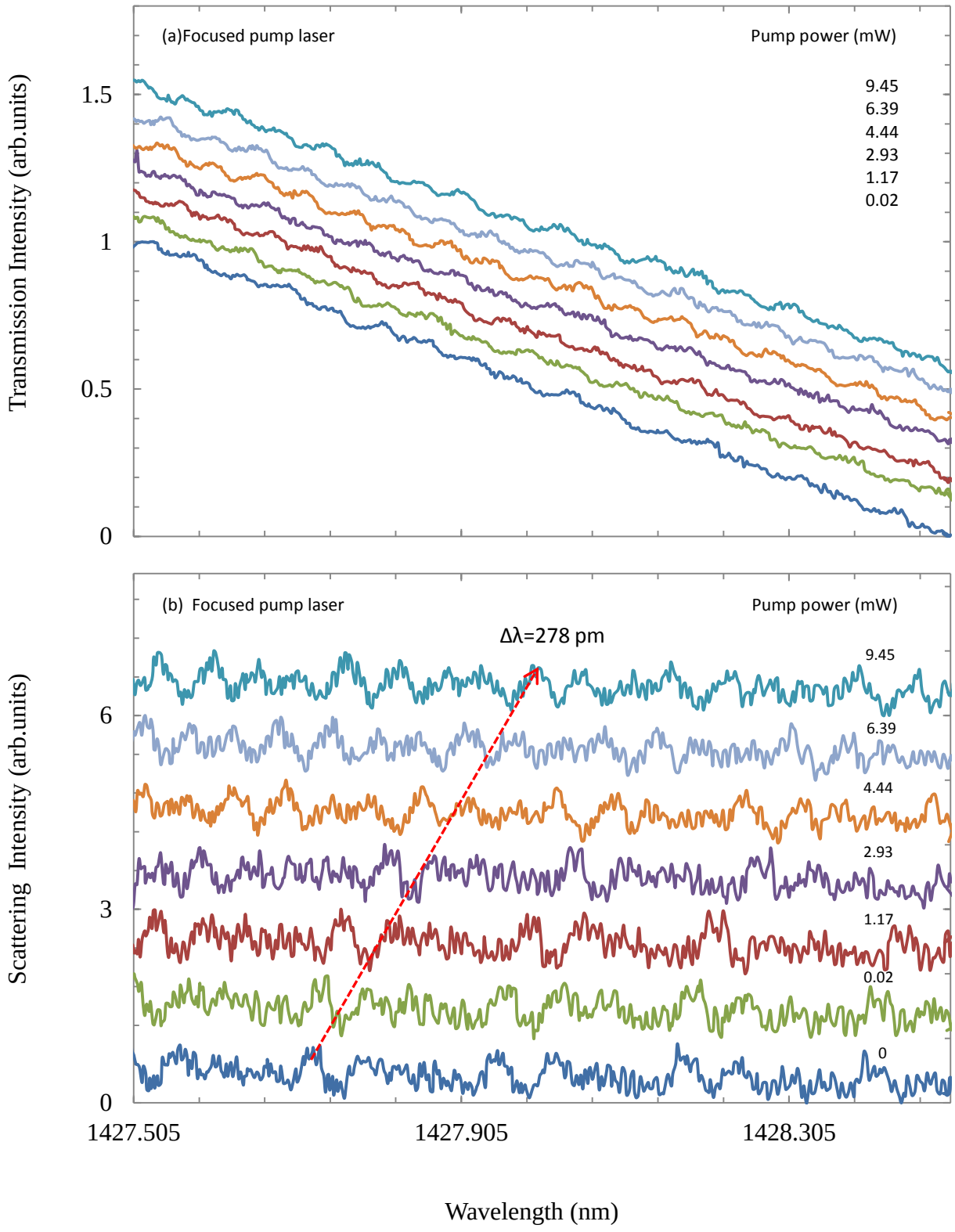

Figure 4.10: Focused CW pump intensity dependence of (a) transmission and (b) scattering.

4.5 Pump excitation summary

Pump laser	**Pump laser**	**WGM shift**	**Temperature change**	**Pump intensity**	**Scattering figure**
variable	-	$\Delta\lambda$	T	I	#
unit	-	pm	K	mW/cm^2	#
Fixed CW at max. power	unfocused	13.5	0.177	1125.5	8
	focused	24.5	0.32	9760.8	9
Pulsed max. power	unfocused	40	0.52	1411.52	11b
	focused	NA	NA	15217	12b
Variable CW at max power	unfocused	97	1.24	1125.5	13b
	focused	278	3.58	9760.8	14b

Table 4.3: Summary of WGM red shifts as a function of pump parameters.

The summary of the observed cases is tabulated in below Table 4.3. We have performed the CW and pulse mode pump excitation for the study of thermo-optic effect (TOE) in a silicon microsphere. The study shows that at low frequency pump excitation we can achieve significant shift of the WGM. The CW pump excitation with ND filters yield more shift than the shift observed with normal on/off CW case, and it is because of the modulation geometry, which needed to be change with the installation of filter wheel.

Chapter 5

CONCLUSIONS

To conclude, we have shown the optical tuning of the whispering gallery modes (WGMs) of a silicon microsphere. We started with the motivation behind silicon photonics and the use of resonant structures for enhancing nonlinearities in silicon. The optical effects in silicon which includes charge carrier effects, optical Kerr effect, one photon absorption (OPA), two photon absorption (TPA), free carrier absorption (FCA), free carrier dispersion (FCD), and the thermo-optic effect (TOE) are discussed. We particularly discussed thermo-optic effect (TOE) in detail as it is the effect of subject in this study. The optical WGMs are further discussed including the potential of WGM resonators which are already exploited in photonics and the theory. In the theory, we have discussed the formation of WGM, the spectral properties, and the different technique, which are used to couple light to microresonators. Finally the proposed work is discussed in detail as follows.

We performed the tuning of the refractive index of a silicon microsphere of 500 μm in response to high absorption at 405 nm. The refractive index is tuned at ms regime which makes the thermooptic effect dominant. When the pump is in CW mode and the beam is unfocused, the amount of red shift in the WGM spectra is 13.5 pm, and for the focused beam the WGM red shift of 24.5pm is observed. When pump is used in pulse mode with unfocused beam, the WGM shifts by maximum of 40 pm (at 80% of pump duty cycle). Further changing the pump power in CW yields 97 pm of red shift for the unfocused beam and 278 pm of red shift for the focused beam. In summary we demonstrated that the WGMs of a silicon microsphere can be tuned optically,

and the analysis provides the base for the realization of all optical switching in a silicon microsphere.

As for the future work, we suggest the ultrafast all optical effect of a silicon microsphere which would enable the observation of high order nonlinear effects, e.g., Kerr effect, Raman effects with the similar setup. To better see the amount of WGM shift for the case of much intense pump, we can perform the experiment for a relatively bigger probe wavelength window. We also suggest performing the experiment for angle dependent tuning of the refractive index of the microsphere, which would allow the study of any changes to polar modes due to azimuthal modes of the microsphere.

VITA

Imran Khan completed his secondary school education from Federal Government Boys High School Quetta Cantt and higher secondary school education from Federal Government Degree College Quetta Cantt. After which he got information communication technology research and development (ICTR&D) scholarship by the Ministry of Information Technology Pakistan for BS (Hons.) in Telecommunication Engineering at National University of Computer and Emerging Sciences Pakistan in 2011. His final year project was based on electroencephalogram (EEG) signals with title "Brain Computer Interface Based System for People with Locked in Syndrome", where he demonstrated a communication system which enabled people to type text with their thoughts only. He won 2nd prize for that work at National Level Engineering Projects Competition in 2011 at COMSATS University, Abbottabad.

After completing his bachelor's degree, he joined Nayatel Pvt. Ltd. as Operations Engineer in the transmission department, where he was leading a team of fiber to the home (FTTH) installations and served the company for one year and four months.

In September 2013 he joined Koç University Microphotonics Research Laboratory under the supervision of Prof. Ali Serpengüzel. At Koç University, he studied as both teaching and research assistant at the Department of Physics. During his MSc, he worked on silicon microspheres and performed the work titled "Optical Tuning of the Whispering Gallery Mode Resonance of a Silicon Microsphere" towards the thesis requirement of the MSc degree. He successfully defended his thesis on 8 Sep 2015.

BIBLIOGRAPHY

[1] B. Jalali and S. Fathpour, "*Silicon Photonics*", Journal of Lightwave Technology, Vol. 24, No. 12, 4600-4615, (2006).

[2] N. Izhaky, M. T. Morse, S. Koehl, O. Cohen, D. Rubin, A. Barkai, G. Sarid, R. Cohen, and M. J. Paniccia, "*Development of CMOS-Compatible Integrated Silicon Photonics Devices*", IEEE Journal of Selected Topics in Quantum Electronics, Vol. 12, No. 6, 1688-1698 (2006).

[3] Y. A. Vlasov, "*Silicon CMOS-Integrated Nano-Photonics for Computer and Data Communications Beyond 100G*", IEEE Communications Magazine, Vol. 50, No. 2, S67-S72 (2012).

[4] L. T. Canham, "*Silicon quantum wire array fabrication by electrochemical and chemical dissolution of wafers*", Applied Physics Letters, Vol. 57, No. 10, 1046-1048 (1990).

[5] D. D. D. Ma, C. S. Lee, F. C. K. Au, S. Y. Tong, S. T. Lee, "*Small-Diameter Silicon Nanowire Surfaces*", Science, Vol. 299, No. 5614, 1874–1877 (2003)

[6] J. Zhu, Z. Yu, G. F. Burkhard, C.-M. Hsu, S. T. Connor, Y. Xu, Q. Wang, M. McGehee, S. Fan, and Y. Cui, "*Optical Absorption Enhancement in Amorphous Silicon Nanowire and Nanocone Arrays*", Nano Letters, Vol. 9, No. 1, pp. 279-282 (2009).

[7] V. Parkhutik, and J. M. M. Duart, "*Analysis of electrical and optical properties of Silicon nanoclustersusing flicker-noise spectroscopy*", Applied Organometallic Chemistry, Vol. 15, No. 5, 359–364 (2001).

[8] D. J. Lockwood and L. Pavesi, "*Silicon fundamentals for photonics applications",* Springer Berlin Heidelberg, 2004.

[9] R. A. Soref, "*Silicon-Based optoelectronics*", Proceedings of the IEEE, Vol.81, No.12, 1687-1706 (1993).

[10] M. Loncar, T. Doll, J. Vuckovic, A. Scherer, "*Design and fabrication of silicon photonic crystal optical waveguides*", Journal of Lightwave Technology, Vol. 18, No. 10, 1402–1411 (2000)

[11] T. Tanabe, M. Notomi, S. Mitsugi, A. Shinya, and E. Kuramochi, "*All-optical switches on a silicon chip realized using photonic crystal nanocavities*", Appl. Phys. Lett. Vol. 87, No. 15, 151112 (2005).

[12] C. Koos, P. Vorreau, T. Vallaitis, P. Dumon, W. Bogaerts, R. Baets, B. Esembeson, I. Biaggio, T. Michinobu, F. Diederich, W. Freude & J. Leuthold, "*All-optical high-speed signal processing with silicon–organic hybrid slot waveguides*", Nature Photonics, Vol. 3, No. 4, 216 - 219 (2009).

[13] V. S. Ilchenko, X. S. Yao, and L. Maleki, "Pigtailing the high-Q microsphere cavity: a simple fiber coupler for optical whispering-gallery modes", Optics Letters, Vol. 24, No. 11, 723-725 (1999).

[14] M. K.-Gonokami, R. H. Jordan, A. Dodabalapur, H. E. Katz, M. L. Schilling, and R. E. Slusher, "*Polymer microdisk and microring lasers*", Optics Letters, Vol. 20, No. 20, 2093-2095 (1995).

[15] D. Armani, B. Min, A. Martin, and K. J. Vahala, "*Electrical thermo-optic tuning of ultrahigh- Q microtoroid resonators*", Applied Physics Letters, Vol. 85, No. 22, 5439-5441 (2004).

[16] A. Hache and M. Bourgeois, "*Ultrafast all-optical switching in a silicon-based photonic crystal*" Appl. Phys. Lett. Vol. 77, No. 25 , 4089–4091 (2000).

[17] S. W. Leonard, H. M. van Driel, A. Birner, U. Gösele, "*All-optical ultrafast tuning of two dimensional silicon photonic crystals via free-carrier injection*", "All-optical ultrafast tuning of two-dimensional silicon photonic crystals via free-carrier injection." *Quantum Electronics and Laser Science Conference, 2001. QELS'01. Technical Digest. Summaries of Papers Presented at the*. IEEE, (2001).

[18] V. R. Almeida, A. Barrios, R. Panepucci, and M. Lipson, "*All-optical control of light on a silicon chip*", Nature, Vol. 43, No. 7012, 1083-1084 (2004).

[19] L.-Wee Luo, G. S. Wiederhecker, J. Cardenas, C. Poitras, and M. Lipson, "*High quality factor etchless silicon photonic ring resonators*", Optics Express, Vol. 19, No. 7, 6284-6289 (2011).

[20] A. Biberman, M. J. Shaw, E. Timurdogan, J. B. Wright and M. R. Watts, "*Ultralow-loss silicon ring resonators*", Optics Letters, Vol. 37, No. 20, 4236-4238 (2012).

[21] D. Grassani, S. Azzini, M. Liscidini, M. Galli, M. J. Strain, M. Sorel, J. E. Sipe And D. Bajoni, "*Micrometer-scale integrated silicon source of time-energy entangled photons*", Optica, Vol.2, No. 2, 88-94 (2015)

[22] F. H. Suhailin, N. Healy, Y. Franz, M. Sumetsky, J. Ballato, A. N. Dibbs, U. J. Gibson, and A. C. Peacock1," *Kerr nonlinear switching in a hybrid silica silicon microspherical resonator*", Optics Express, Vol. 23, No. 13, 17263-17268 (2015).

[23] M. Soltani, S. Yegnanarayanan and A. Adibi, "*Ultra-high Q planar silicon microdisk resonators for chip-scale silicon photonics*", Optics Express, Vol. 15, No. 8, 4694-4704 (2007).

[24] "*Silicon (Si)*", University of Reading, Infrared multilayer laboratory, Retrieved 31 August 2015.

[25] N. J. Halas, D. Krökel, and D. Grischkowsky, "*Ultrafast light-controlled optical-fiber modulator*", Applied Physics Letters Vol. 50, No. 14, 886-888 (1987).

[26] S. R. Friberg, A. M. Weiner, Y. Silberberg, B. G. Sfez, and P. S. Smith, "*Femtosecond switching in a dual-core-fiber nonlinear coupler*", Optics Letters, Vol. 13, No. 10, 904-906 (1988).

[27] R. H. Pantell, R. W Sadowski, M. J. F. Digonnet, and H. J. Shaw, "*Laser-diode-pumped nonlinear switch in erbium-doped fiber*", Optics Letters, Vol. 17, No. 14, 1026-1028 (1992).

[28] L. Alloatti, D. Korn, R. Palmer, D. Hillerkuss, J. Li, A. Barklund, R. Dinu, J. Wieland, M. Fournier, J. Fedeli, H. Yu, W. Bogaerts, P. Dumon, R. Baets, C. Koos, W. Freude, and J. Leuthold, "*42.7 Gbit/s electro-optic modulator in silicon technology*", Optics Express, Vol. 19, No. 12, 11841-11851 (2011).

[29] L. Alloatti, R. Palmer, S. Diebold, K. P. Pahl, B. Chen, R. Dinu, M. Fournier, J.-M. Fedeli, T. Zwick, W. Freude, C. Koos and J. Leuthold, "*100 GHz silicon–organic hybrid modulator*", Light: Science & Applications, 3, e173 (2014).

[30] C. A. Barrios, V. R. Almeida, R. Panepucci, and M. Lipson, "*Electrooptic Modulation of Silicon-on-Insulator Submicrometer-Size Waveguide Devices*", Journal Of Lightwave Technology, Vol. 21, No. 10 , 2332 (2003).

[31] F. Gan and F. X. Kärtner, "*High-Speed Silicon Electrooptic Modulator Design*", IEEE Photonics Technology Letters, Vol. 17, No. 5, 1007-1009 (2005).

[32] X. Ma and G.-Sheng, "Optical Switching Technology Comparison: Optical MEMS vs. Other Technologies", IEEE Optical Communications, Vo. 41, No. 11, s16- s23 (2003).

[33] X. Sang, E.-K. Tien, and O. Boyraz, "*Applications of two-photon absorption in silicon*", Journal of Optoelectronics and Advanced Materials, Vol. 11, No. 1, 15 – 25 (2008).

[34] D. E. Houston, S. Krishna, and E. D. Wolley, "*Study of charge dynamics in high speed power devices using free carrier absorption measurements*", Electron Devices Meeting, 1976 International IEEE, Vol. 22, 504-507 (1976).

[35] W. Denk, Winfried, W. W. Webb, and J. H. Strickler, "*Two-photon laser scanning fluorescence microscopy*", *Science*, Vol. 248, No. 4951, 73-76 (1990).

[36] Q. Xu and M. Lipson, "*All-optical logic based on silicon micro-ring resonators*", Optics Express, Vol. 15, No. 3, 924-929 (2007).

[37] D.-X Xu, "Polarization control in silicon photonic waveguide components using cladding stress engineering" in the text book of Silicon Photonics II Components and Integration, ed. II, Ed. D. J. Lockwood and L. Pavesi, Springer (2011).

[38] V. Loriot, E. Hertz, O. Faucher & B. Lavorel, "*Measurement of high order Kerr refractive index of major air components*", Optics express, Vol. 17, No. 16, 13429-13434 (2009).

[39] R. A. Soref, and B. R. Benett, "*Electrooptical effects in Silicon*" IEEE Journal of Quantum Electronics, Vol. 23, No. 1, 123–129 (1987).

[40] D. A. Clugston and P. A. Basore, "*Modelling Free-carrier Absorption in Solar Cells*", Progress in Photovoltaics: Research and Applications, Vol. 5, 229-236 (1997).

[41] P. E. Schmid, "*Optical absorption in heavily doped silicon*", Physical Review B, Vol. 23, No. 10, 5531 (1981).

[42] D. K. Schroder, R. N. Thomas, And J. C. Swartz, "*Free Carrier Absorption in Silicon*", IEEE Journal Of Solid-State Circuits, Vol. 13, No. 1, 180-187 (1978).

[43] S. C. Jain, A. Nathan, D. R. Briglio, D. J. Roulston, C. R. Selvakumar, and T. Yang, "*Band-to-band and free-carrier absorption coefficients in heavily doped silicon at 4 K and at room temperature*", Journal of Applied Physics, Vol. 69, No. 6, 3687-3690 (1991).

[44] R. de. L. Kronig, "*On the theory of dispersion of X-Rays*", Journal of Optical Society of America, Vol. 12, No. 6, 547-557 (1926).

[45] S. Hassing and O. S. Mortensen, "*Kramers-Kronig relations and resonance raman scattering*", The Journal of Chemical Physics, Vol. 73, No. 3, 1078-1083 (1980).

[46] B. J. Li, "*Electro-optical switches*", in the Optical Switches: Materials and Design, S.-J. Chua and B. J. Li, Eds., Elsevier, 2010.

[47] F. G. D. Corte, M. E. Montefusco, L. Moretti, I. Rendina, and G. Cocorullo, "*Temperature dependence analysis of the thermo-optic effect in silicon by single and double oscillator models*" Journal of Applied Physics, Vol. 88, No. 12, 7115-7119 (2000).

[48] M. K. Davis and M. J. F. Digonnet, "*Nanosecond Thermal Fiber SwitchUsing a Sagnac Interferometer*" IEEE Photonics Technology Letters, Vol. 11, No. 10, 1256-1258 (1999).

[49] L. L. Martín, C. P. -Rodríguez, P. H.-González, and I. R. Martín, "*Whispering gallery modes in a glass microsphere as a function of temperature*", Optics Express, Vol. 19, No. 25, 25792-25798 (2011).

[50] H. C. Tapalian., J-P. Laine, and P. A. Lane. "*Thermooptical switches using coated microsphere resonators*", Photonics Technology Letters, IEEE, Vol. 14, No. 8, 1118-1120 (2002).

[51] A. Tewary, M. J. F. Digonnet, and M. L. Brongersma, "*Silicon-nanocrystal-coated Silica Microsphere Thermooptical Switch",* IEEE Journal Of Selected Topics In Quantum Electronics, Vol. 12, No. 6, 1476-1479 (2006).

[52] T. J. Johnson, M. Borselli, and O. Painter, "*Self-induced optical modulation of the transmission through a high-Q silicon microdisk resonator*", Optics Express, Vol. 14, No. 2, 817-831 (2006).

[53] A. G. Fox and T. Li, "*Resonant Modes in a Maser Interferometer*", Bell System Technical Journal, Vol. 40, No. 2, 453–488 (1961).

[54] G. D. Boyd and J. P. Gordon, "*Confocal Multimode Resonator for Millimeter Through Optical Wavelength Maser*", Bell System Technical Journal, Vol. 40, No. 2, 489–508 (1961).

[55] L. Rayleigh "*The problem of the whispering gallery*" Philosophical Magazine Series 6, Vol. 20, No. 120, 1001-1004 (1910)

[56] C. Righini, Y. Dumeige, P. Feron, M. Ferrari, G. Conti, D. Ristic, S. Soria, "*Whispering gallery mode microresonators: Fundamentals and applications",* Societa Italiana di Fisica, Vol. 34, No. 7 (2011).

[57] V. B. Braginsky, M. L. Gorodetsky, and V. S. Lichenko, "*Optical whispering-gallery microresonators*", SPIE Vol. 2097 Laser Applications, 283-288 (1994).

[58] M. Cai, G. Hunzeker, and K. Vahala, "*Fiber-Optic Add–Drop Device Based on a Silica Microsphere-Whispering Gallery Mode System*", IEEE Photonics Technology Letters, Vol.11, No.6, 686-687 (1999).

[59] F. Vollmer and S. Arnold, "*Whispering-gallery-mode biosensing: label-free detection down to single molecules*", Nature Methods, Vol. 5, No. 7, 591-596 (2008).

[60] H. C. Tapalian, J.-P. Laine, and P.A. Lane," *Thermooptical Switches Using Coated Microspher Resonators*", IEEE Photonics Technology Letters, Vol.14, No.8, 1118-1120 (2002).

[61] Y. Yao & J. Yao, V. K. Narasimhan, Z. Ruan, C. Xie, S. Fan, and Y. Cui, "*Broadband light management using low-Q whispering gallery modes in spherical nanoshells*", Nature Commmunications, Vol. 3, 664 (2012).

[62] H. –G. Park, J.-K. Hwang, J. Huh, H.-Y. Ryu, S.-H Kim, J. -S Kim, and Y. -H Lee, "*Characteristics of Modified Single-Defect Two-Dimensional Photonic Crystal Lasers*", IEEE Journal Of Quantum Electronics, Vol. 38, No. 10, 1353-1365 (2002).

[63] P.-T. Lee, T.-Wen Lu, J.-H. Fan, and F.-M. Tsai, "*High quality factor microcavity lasers realized by circular photonic crystal with isotropic photonic band gap effect*", Applied Physics Letters, Vol. 90, No. 15, 151125 (2007).

[64] A. Serpengüzel, A. Kurt, and U. K. Ayaz, "*Silicon microsphere for electronic and photonics integration*", Photonic and Nanostructures Fundamentals and Applications, Vol.6, No. pp. 179-182 (2008).

[65] A. Serpengüzel, S. Arnold, G. Griffel and J. A. Lock, "*Enhanced coupling to microsphere resonances with optical fibers*", J. Opt. Soc. Amer. B, Opt. Phys., Vol. 14, no. 4, 790-795 (1997).

[66] P. C. Chaumet, A. Rahmani, F. de Fornel, and J. P. Dufour, "*Evanescent light scattering: The validity of the dipole approximation*", Physical Review B, Vol. 58, No. 4, 2310 (1998).

[67] A. C. R. Pipino, J. W. Hudgens, and R. E. Huie, "*Evanescent wave cavity ring-down spectroscopy with a total-internal-reflection minicavity*", Review of Scientific Instruments, Vol. 68, No. 8, 2978-2989 (1997).

[68] P. Chýlek, "*Partial-wave resonances and the ripple structure in the Mie normalized extinction cross section*", Journal of Optical Society of America, Vol. 66, No. 3, 285-287 (1976).

[69] H.-B. Lin, A. L. Huston, J. D. Eversole, and A. J. Campillo, "*Internal scattering effects on microdroplet resonant emission structure*", Optics Letters, Vol. 17, No. 14, 970-972 (1992).

[70] P. Chylek, J. T. Kiehl, and M. K. W. Ko, "*Optical levitation and partial-wave resonances*", Physical Review A, Vol. 18, No. 5, 2229 (1978).

[71] B. Rayleigh, John William Strutt, Scientific papers, University Press (Cambridge) (1920)

[72] C. C. Lam, P. T. Leung, and K. Young, "*Explicit asymptotic formulas for the positions, widths, and strengths of resonances in Mie scattering*", Journal of the Optical Society of America B, Vol. 9, No. 9, 1585-1592 (1992).

[73] J. R. P.-Jones, "*Resonance component of backscattering by large dielectric spheres*", Journal of Optical Society of America, Vol. 1, No. 8, 822-830 (1984).

[74] L. Shi, R. Fenollosa, T. U. Tuzer and Francisco Meseguer, "*Angle-Dependent Quality Factor of Mie Resonances in SiliconColloid-Based Microcavitie*s", ACS Photonics, Vol. 1, No. 5, 408−412 (2014).

[75] M. L. Gorodetsky, A. A. Savchenkov, and V. S. Ilchenko, "*Ultimate Q of optical microsphere resonators*", Optics Letters, Vol. 21, No. 7, 453-455 (1996).

[76] V. S. Ilchenko, , A. A. Savchenkov, A. B. Matsko, and L. Maleki, "*Generation of kerr frequency combs in a sapphire whispering gallery mode resonator*", Optical Engineering, Vol. 53, No. 12, 122607-122607 (2014).

[77] A. J. Cox and Dean C. Dibble, "*Nondiffracting beam from a spatially filtered Fabry-Perot resonator*", Journal of Optical Society of America A, Vol. 9, No. 2, 282-286 (1992).

[78] A. Serpengüzel and S. Arnold, "*Excitation of resonances of microspheres on an optical fiber*", Optics Letters, Vol. 20, No. 7, 654-656 (1995).

[79] S. M. Spillane, T. J. Kippenberg, O. J. Painter, and K. J. Vahala, "*Ideality in a Fiber-Taper-Coupled Microresonator System for Application to Cavity Quantum Electrodynamics*", Physical Review Letters, Vol. 91, No. 4, 043902 (2003).

[80] J.-P. Laine, B. E. Little, D. R. Lim, H. C. Tapalian, L. C. Kimerling, and H. A. Haus, "*Microsphere resonator mode characterization by pedestal anti-resonant reflecting waveguide coupler*", IEEE Photonics Technology Letters, Vol. 12, No. 8, 1004-1006 (2000).

[81] P. K. Tien, and R. Ulrich, "*Theory of Prism-Film Coupler and Thin-Film Light Guides*", Journal of the Optical Society of America, Vol. 60, No. 10, 1325-1337 (1970).

[82] A. Serpengüzel, S. Işçi, T. Bilici, and A. Kurt, "*Microsphere-based optical system for biosensor applications*", *Proc. SPIE*5317, Optical Fibers and Sensors for Medical Applications IV, 180 (2004).

[83] Z.-G. Chen and A. Taflove, "*Highly efficient optical coupling and transport phenomena in chains of dielectric microspheres*", Optics Letters, vol. 31, No. 3, 389-391 (2006).

[84] G. Cocorullo, M. Iodice, I. Rendina, and P. M. Sarro, "*Silicon Thermooptical Micromodulator with 700-kHz - 3-dB Bandwidth*", IEEE Photonics Technology Letters, Vol. 7, No. 4, 363-365 (1995).

[85] G. Cocorullo, and I. Rendina, "*Thermo-optical modulation at 1.5μm in silicon etalon*", Electronics Letters, Vol. 28, No. 1, 83-85 (1992).

[86] G. Cocorullo, F. G. D. Carte, I. Rendina, P. M. Sarro, "*Thermo-optic effect exploitation in silicon microstructures*", Sensors and Actuators A, Vol. 71, Vol. 1, 19-26 (1998).

[87] F. H. Suhailin, N. Vukovic, P. Mehta, N. Healy, and A. C. Peacock, "*Kerr nonlinear switching in silicon fibre-based microcylindrical resonators*", in Workshop on Specialty Optical Fibers and their Applications, (Optical Society of America, 2013), paper F2.6.